C.P. No. 942

C.P. No. 942

MINISTRY OF TECHNOLOGY

AERONAUTICAL RESEARCH COUNCIL

CURRENT PAPERS

An Experimental Investigation of the Two-dimensional Wall Jet

James H. Whitelaw

LONDON: HER MAJESTY'S STATIONERY OFFICE

1967

Price 10s 6d net

C.P.No.942*

April, 1966

An Experimental Investigation of the Two-dimensional Wall Jet

- By -

James H. Whitelaw

SUMMARY

A new apparatus, designed to investigate the effects of slot geometry on the effectiveness of film cooling, is described and new measurements of the impervious wall effectiveness are presented. The measurements were performed in the range $2.24 \leq m \leq 0.47$ using helium as a tracer gas and gas chromatographic equipment to detect the relevant concentrations. The appropriate hydrodynamic quantities are reported in detail.

Contents/

---

* Replaces: Imperial College/HRJ/36 - A.R.C.28 179

Contents

1. Introduction

Previous experimental investigations of wall jets [1,2,3,4 and 5] indicate that the adiabatic wall effectiveness of the film cooling process is considerably affected by the geometry of the injection region. The slot geometries employed by the authors of references 1 to 5 range from a simple two-dimensional slot to an injection region made up of a series of holes in line and, for the same mass flow rate through the slot and for similar free stream velocities, the measured values of the adiabatic wall effectiveness at locations downstream of the slot differ by hundreds of percent. These differences may be attributed to a variety of variables, for instance, three dimensional flow, free stream turbulence, jet turbulence, density gradients etc. It is not possible to separate these effects from the reported data.

Many investigations of the adiabatic wall effectiveness have been carried out using simple, two-dimensional slot configurations [6,7,8,9,10, 11,12,13 and 14] and under conditions which would suggest that the effect of three dimensional flow, free stream turbulence, etc. would be small. Nevertheless, discrepancies of the order of 100% exist and, although the variables mentioned above may play some part in explaining these discrepancies, it is likely that the various geometric configurations of the injection region are a principal cause. A critical review of the existing experimental data with particular reference to the geometry of the injection region is contained in reference 15. This review suggested the need for a systematic investigation of the effects of slot geometry using a single apparatus in order to eliminate the spurious effects which stem from analysing data obtained on different apparatus.

The present report has two main purposes:

(i) to describe new apparatus designed to carry out an investigation of the effects of slot geometry and the techniques which are being employed to obtain the necessary measurements.

(ii) to present new values of effectiveness, obtained from concentration measurements on an impervious wall, and the corresponding values of the relevant hydrodynamic quantities. The measurements of the impervious wall effectiveness are directly comparable with values of adiabatic wall effectiveness if the turbulent Lewis number is unity - this possibility is discussed in section 5.5. For the purposes of the present investigation, however, it is not important for the two to be identical since the measurements reported here will be compared with later measurements which will be performed with different slot geometries but using the same mass transfer technique.

The detailed hydrodynamic data reported here, were measured for two main reasons. The first was to determine the properties of the wind tunnel and to ascertain its advantages and disadvantages. The second was to provide an empirical relationship between the slot properties and those at some location downstream of the slot. Such a relationship is necessary if a method of predicting the effectiveness is to be developed from a theory involving integral equations, such as that of D. B. Spalding [16].

2. Description of the Wind Tunnel

The wind tunnel designed for the present investigation can conveniently be described in three sections, i.e. the fan, the expansion-contraction section and the working section.

The fan was manufactured by Carter Thermal Engineering Ltd. (Gyro flow fan, size $24\frac{1}{4}$", arrangement 1) and is capable of delivering 10 000 ft ^{3}/min against a pressure head of 8 inches of water when running at a speed of 1920 rpm. The fan was chosen to run as a blower since this results in the static pressure in the working section being close to atmospheric. Adjustment of the fan speed, and hence of the working section free stream velocity, is achieved by changing the fan or motor pulley wheel. These pulley wheels are of the variable radius type and hence a 15 - 25% reduction of speed is obtainable without removing the pulley wheels. Before entering the fan, the incoming air is filtered through a surface area of approximately 70 ft^2 of felt.

The delivery side of the fan is of rectangular section $2' - 0\frac{1}{2}" \times 1' - 9\frac{1}{2}"$. This is expanded to a rectangular cross-section of 48" x 32" in a distance of 2' - 11", maintained at this cross-section for a distance of 9" and then contracted to the dimensions of the working section, i.e. 18" x 12", over a distance of 4' - 9". The form of the contraction from 4' - 0" to 18' was copied from a similar tunnel in the Aeronautical Engineering Department of Imperial College and the form of the 2' - 8" to 12" contraction was scaled from the former. Table 1 gives the dimensions of the contraction. The expansion-contraction section was constructed from wood by A. B. Fuller Ltd.

These copper screens were located in the expansion-contraction section, all three being 20 mesh, 28 swg. One was located at each end of the 4' - 0" x 2' - 8" section and one half way along the expansion sectior.

The working section was manufactured in the Mechanical Engineering Workshop of Imperial College. It is 6' - 0" long, has an 18" x 12" cross-section and was manufactured from Dural and Perspex. The top plate of the working section is split into two, allowing a 4" gap to run 5' - 4" along the length of the tunnel. The traversing equipment slides in this gap and can be firmly secured at any location along this length. The resulting open sections are closed with a variety of lengths of Dural plate which locate positively in the gap.

The traversing equipment allows a total head probe (or hot wire probe) to be traversed along a 5' - 4" length of the working section, over a 3" width of the working section ($1\frac{1}{2}$" on each side of the centre line) and over a distance of up to 4" from the top surface of the base plate: only a small modification is required to extend this 4" to the full 12" height of the working section.

The base plate of the working section is made from $\frac{1}{2}$" thick Dural and has a large number of 0.020" holes drilled in it as shown in figure 1. These holes serve as static pressure taps or, as we shall see later, as sampling holes through which samples of the air close to the wall

can be extracted. The plate can be adjusted to ensure that the gradient of static pressure in the tunnel is zero or to impose a linear pressure gradient on the flow.

On the same frame as the working section, the secondary fan (Sturtevant 3 Heavy Duty Monogram Fan) and motor are mounted. The air from this fan is directed into an 18" x 9" x 28" plenum chamber before discharging through a slot at the leading edge of the base plate of the working section. This is shown diagrammatically in figure 2. The slot can readily be changed or replaced by an insert which permits the flow to conform to the usual flat plate boundary layer. A pressure gradient can be imposed upon the flow by adjustment of the tunnel base plate. The flow from the secondary blower is again controlled by means of the pulley wheels on the fan and motor shafts but in this case there is also a slide plate on the pressure side of the fan. A filter box is attached to the suction side of the fan, the incoming of air having to pass through an area of 25 ft^2 of felt.

3. Hydrodynamic Measurements on a Flat Plate

In order to test the performance of the traversing equipment, the total head probe and the tunnel itself, the secondary air stream was blanked off and velocity profiles recorded with a flat plate boundary layer configuration. The static pressure gradient along the working section was arranged to be sensibly zero by adjusting the tunnel base plate. The boundary layer was arranged to have a leading edge at entry to the working section by having the base plate above the level of the lower surface of the contraction and preceding this base plate by a splitter plate.

Velocity profiles were measured at two values of x, the distance downstream of the leading edge. These profiles are shown in figure 3 which graphs the value of u^+ against y^+ on semi-logarithmic coordinates. Also shown on this figure are the line

$$u^+ = \frac{1}{0.41} \ln (7.7y^+) \qquad \ldots \quad 3.1$$

and the curve

$$u^+ = y^+ \qquad \ldots \quad 3.2$$

These equations represent the Universal Velocity profile, the former being valid in the region $y^+ > 30$ and the latter in the region $y^+ < 5$. It should be stressed that the Universal Velocity profile is not sufficiently universal for the constants 0.41 and 7.7 in equation 3.1 to be considered as exact. A variety of values for these constants have been suggested in the past and the values used here fit the available experimental data as well as most. In order to locate the measured points on this curve it was necessary to determine the value of the dimensionless wall shear stress. This was done in the manner suggested by Clauser [17] i.e., by plotting the data on a graph of u/u_G against $u_G y/\nu$, lines of constant shear stress, $c_f/2$, having previously been drawn on the graph with the aid of equation 3.1. In this way the following values of $c_f/2$ were obtained:

$R_x = 2.83 \times 10^6 \quad c_f/2 = 0.00182 \quad (0.00196)$
$R_x = 9.4 \times 10^5 \quad c_f/2 = 0.00220 \quad (0.00236)$

These/

These may be compared with the values given in parenthesis which were obtained with the aid of the equation

$$c_f/2 = 0.037 \; R_x^{-1/5} \qquad \ldots 3.3$$

derived on the assumption of a $\frac{1}{7}$ power profile [18].

The values of shear stress given above and the experimental data plotted on figure 3, indicate that the apparatus and the experimental techniques are generally satisfactory. Two specific points arise out of the data shown in figure 3. Firstly, a smooth curve drawn through the experimental points for the measurement at an R_x value of 2.83×10^6 would indicate an increase above the line represented by equation 3.1 in the range $20 < y^+ < 60$. Earlier measurements, made with a total head probe which was supported less rigidly than the one used for the present measurements, indicated an even greater increase above the line represented by equation 3.1. Similar curves have been reported by Townsend [19], Bradshaw and Ferriss [20] and Patel [21]. Bradshaw and Ferriss suggested that the reason for the experimental data being higher than might be expected from the requirement $\tau = \tau_w$, is the effect of turbulent fluctuations on the total head probe. The present measurement would support this conclusion since the stiffening of the probe, and hence the reduction in amplitude of the vibration of the probe tip, resulted in a decrease in this rise in the curve.

It should be noted at this point that no displacement correction has been applied to the data shown in figure 3. A correction of the form 0.15 $\underline{d}$, where $\underline{d}$ is the tip height of the total head probe, can be partly justified (see, for example references 22 and 23) and would tend to remove the rise in the curve. However, the justification for the correction does not appear to be complete and consequently it has not been applied. In the measurements presented in figure 3, and for the subsequent velocity measurements of this paper, the total-head probe tip dimensions were:

outside: 0.063" × 0.0096"

inside: 0.053" × 0.0036"

Thus a displacement correction of the order of 0.15 $\underline{d}$ would not be sufficient to remove the rise in the curve.

The second point which arises out of figure 3 is the tendency of the data at the Reynolds number, R_x, of 9.4×10^5, to increase monotonically above the line represented by equation 3.1. for values of y^+ less than 100. This is the result one might expect from plotting the variables u^+ and y^+, both of which involve a constant value of shear stress, for a boundary layer which is not fully turbulent. The magnitude of the Reynolds number, i.e. $R_x = 9.4 \times 10^5$, would also suggest that the boundary layer was not fully turbulent at this value.

It was considered that the results described above indicated that both the equipment and the experimental techniques are reliable, in that they are capable of reproducing accepted measurements for flat plate boundary layers.

4./

4. Hydrodynamic Measurements on a Flat Plate with Tangential Injection

Two similar, but slightly different slot geometries have been used in the present series of experiments. Both are shown diagrammatically in figure 4. The slot shown in figure 4a was used for the preliminary measurements required to test the performance of the equipment with secondary injection. These data are reported in Table 2. The data reported in Table 3 were obtained using the slot shown in figure 4b.

No major problems were encountered in making the velocity profile measurements. It was discovered that, with a slot height of approximately 0.25", a slot velocity of 180 ft/s could not be exceeded due to leaks caused by the pressure in the secondary system. No attempt was made to eliminate these leaks at 180 ft/s. Instead, the slot velocity was always kept below this figure and no significant leaks were observed for these lower velocities. The two-dimensionality of the tunnel and of the slot flow were checked on several occasions at different values of x and y by recording velocities over a 3" span of the tunnel. No significant velocity difference could be detected.

It does not seem necessary in this paper to present diagrammatically all the data tabulated in Tables 2 and 3. However, in order to demonstrate the trends of the measurements and to indicate the experimental precision, it does seem desirable to present some data in graphical form. Consequently, figures 5, 6 and 7 have been prepared and present the quantities R_2, H_{12} and $c_f/2$, respectively, plotted against the dimensionless distance, x/y_c for several experimental runs which were selected to demonstrate the variation of R_2, H_{12} and $c_f/2$ over a wide range of the parameter m. The smooth curves shown on figures 5, 6 and 7 do not represent predictions. They are smooth lines drawn through the experimental points.

It may be seen from figure 5 that the values of dR_2/dR_x for runs 1, 2 and 3 are in agreement with the value of $c_f/2$ shown on figure 7 although there are deviations from the smooth line of up to 7%. For the other runs, however, the values of dR_2/dR_x, at downstream positions, do not agree well with the appropriate value of $c_f/2$ and it is doubtful if the pressure gradient term or the divergence term could account for the discrepancies. It is likely that the reason for the discrepancies is two-fold: first, the general difficulty in obtaining accurate measurements of R_2 and secondly, the tendency of the slot velocity to decrease with time. It has been observed that the slot velocity decreases by up to approximately 5% in the time taken to measure the velocity profiles for any particular run - the percentage decrease, decreases with increasing slot velocity and is negligible for the higher slot velocity runs.

It is also possible that the values of R_2 measured at x/y_c of 10 (and in some cases of 20) are subject to some inaccuracy since the velocity profiles exhibit a minimum. It is also likely that these profiles will not be well represented by two parameters.

Figure 6 demonstrates the trends of the shape factor, H_{12}, for the same experimental runs as are shown on figures 5 and 7. It may be seen that the value of H_{12} becomes singular for run 4 and that this

occurs/

occurs when the value of the Reynolds number, R_2, is small. This presents a mathematical difficulty if an integration procedure is devised, using H_{12} (or H_{32}) as dependent variable, for a flow which transcends from a negative value of R_2 to a positive one. Details of a procedure to overcome this difficulty may be found in reference 24.

It may be seen from figure 7 and from table 3, that some values of the dimensionless shear stress, $c_f/2$, have been omitted. All of the values of $c_f/2$ were obtained by plotting the experimental values of the velocity ratio, u/u_G, against the Reynolds number $u_G y/\nu$, and drawing lines of constant shear stress based upon equation 1 on the same graph. The resulting profiles, if they are of the 'Universal' form, have a portion of their length which lies along one of the lines of constant shear stress, thereby indicating the value of the shear stress which is assumed constant over the inner region of this profile. The values of u/u_G and $u_G y/\nu$ for run 4 are shown plotted in figure 8 and it may be seen that for low values of the dimensionless distance, x/y_C, the profiles have a slope which is always different from that indicated by the lines of constant shear stress. Thus for these runs it is not possible to evaluate a value of shear stress from the data with satisfactory precision. The data of run 4 were chosen for figure 8 because they show the development of a wall jet towards a conventional boundary layer flow for which the velocity, u, is at no time greater than the free stream velocity, u_G. The trend indicated on figure 8 was, however, also shown by the velocity profiles obtained for other runs. In some cases (notably for the lower slot velocities), a value of the dimensionless shear stress could not be determined precisely for values of the dimensionless distance, x/y_C, less than 40. This is probably due, at least in part, to the wall layer still being transitional, i.e. the wall layer has not developed to a fully turbulent form.

It may also be seen from figure 8, that the region of each profile (for $x/y_C \geq 40$) which is parallel to, or coincident with, a line of constant shear stress is short and in some cases very short. This makes it difficult to ascribe a value of shear stress to a particular profile with certainty. However, the values of dimensionless shear stress read from figure 8, and from similar figures are consistent, as shown from figure 7. In addition, these values have been shown to agree well with theory [24] although the measured values do tend to be lower than the predicted values.

It should be noted that in all of the measurements with tangential injection reported in this paper, the boundary layer on the upper edge of the slot was that equivalent to a flat plate boundary layer which had grown from a stagnation point approximately 7" upstream of the lip of the slot.

4.1 Initial conditions necessary for integration procedures

The integration of the integral momentum equation or integral mean kinetic energy equation requires initial conditions and usually values of R_2 and H_{12} are provided at some value of the independent variable R_x. However, any two of the properties R_1, R_2, H_{12}, H_{32} and $c_f/2$ may be chosen at the given value of R_x. In the case of wall jet

flows/

flows it is desirable to be able to predict the value of the initial conditions based upon bulk flow measurements and the slot geometry and usually these initial conditions are required at a value of R_x which is downstream of the end of the potential core region (i.e. the region where the slot velocity u_c is preserved).

Inspection of the definitions of the Reynolds numbers R_1, R_2 and R_3 reveals that, for a given systematic uncertainty in the measured velocity ratio, u/u_c, the error in the Reynolds number increases with its order for jet-like flows and decreases for flows with no velocity maximum and high values of u/u_c. Thus the choice of R_2 would seem to be generally more satisfactory than R_1 or R_3.

The choice of the shape factor, H_{12}, leads to a difficulty which is demonstrated by figure 9. At values of the parameter, m, close to unity the value of H_{12} becomes singular in a similar way to that demonstrated by run number 4 on figure 6. Again this occurs when the value of the Reynolds number R_2 tends to zero and, it is possible that this phenomenon can be disregarded and a smooth line drawn to connect the curves on either side of m = 1. This possibility is examined in reference 24 and confirmed. A similar difficulty may be expected with the use of the shape factor H_{32} which is also shown on figure 9. The data obtained by Nicoll [25] are shown on figure 9 and lend general support to the present measurements. Nicoll's measurements were obtained with an essentially rectangular slot velocity profile, in contrast to the present measurements, and this would indicate that the curves presented in figure 9 may apply to all simple, two-dimensional slots. Further measurements are required to support this suggestion.

The dimensionless shear stress, $c_f/2$, might be chosen as a suitable initial value. It should be remembered, however, that for the present measurements, $c_f/2$ was obtained by plotting the velocity profiles on a Clauser plot and that for low values of the ratio, x/y_c, and for low values of the parameter, m, the resulting shear stress values are subject to some uncertainty. If the shear stress had been obtained by direct measurement (assuming that this is more precise than the present method, and this is frequently not the case) then $c_f/2$ would be a suitable property for use as an initial condition.

The above discussion suggests that R_2 and R_1 or R_3 should be used as initial conditions although it may be equally satisfactory to substitute either of the shape factors for R_1 or R_3. Figures 10 and 11 show the present data for R_1 and R_2, together with that of W.B. Nicoll [25], plotted to take account of the slot Reynolds number. It may be seen that the data are well represented by the smooth curves. A similar plot for R_3 is not shown here because the scatter in R_3 appeared to be slightly higher than that of R_1 and R_2. No attempt has been made, at the present time, to formalise these correlations in the form of equations or to test their validity with respect to the present measurement or to measurements obtained with slightly different slot configurations. It is intended that this will be done in the near future.

4.2/

4.2 Turbulence intensity

The effect of free stream and of jet turbulence on the adiabatic wall effectiveness is quantitatively unknown although for cases where the jet velocity is of the same order of magnitude as the free stream velocity, it represents the principal mechanism for mixing. For this reason it seemed desirable to measure turbulence profiles close to the slot and at velocity ratios close to unity. Two series of measurement were made; the first, for a value of the parameter m of 1.62 and at a value of x as close to the slot as was practical, is presented in figure 12 and the second, for a value of the parameter m of 0.852 and at three stations downstream of the slot is presented in figure 13. These measurements were effected using a Disa, constant temperature, hot wire anemometer.

Little need be said about these measurements at the present time. It remains to compare future measurements made with the same value of the parameter m, the same mainstream velocity etc. but with a substantially different slot turbulence profile to determine the downstream effects of the turbulence intensity. It is useful, however, to note the rapid decay of the turbulence intensity in the downstream direction, as demonstrated by figure 13.

5. The Measurement of the Impervious Wall Effectiveness

The purpose of the present program of research is to investigate the effects of the slot geometry on the value of the adiabatic wall effectiveness downstream of the slot. However, as has previously been pointed out, it is equally satisfactory to investigate the effects of slot geometry on the effectiveness based upon mass transfer measurements i.e., the impervious wall effectiveness.

The adiabatic wall effectiveness is usually defined in terms of the conserved property, h, i.e., the specific enthalpy, and if constant fluid properties are assumed, this definition becomes

$$\eta = \frac{T_W - T_G}{T_C - T_G}$$

where T is temperature. The great majority of past measurements of effectiveness have been effected by measuring the temperatures at the W, G and C states.

There are two drawbacks to the use of temperature as a conserved property -

(i) in the determination of the adiabatic wall effectiveness the wall should be adiabatic but all practical walls have a finite conductivity and hence are never truly adiabatic.

(ii)/

(ii) a temperature difference is required between the primary and secondary flows. This temperature difference must be large enough to permit accurate measurements at downstream locations but small enough so that property variations (e.g., density gradients) can be ignored. A satisfactory balance between these two requirements is not easily attained.

Consequently, it was decided to use mass conservation - instead of enthalpy conservation - to determine the effectiveness. This implies the use of mass concentration for the conserved property in the definition of effectiveness.

$$\text{i.e.,} \quad \eta = \frac{m_W - m_G}{m_C - m_G}$$

where m_C refers to the mass concentration of a tracer gas at the slot, m_G refers to the mass concentration of the tracer gas in the free stream and m_W refers to the mass concentration of the tracer gas at the wall at any downstream location. The mass concentration, m_G, may be arranged to be zero and the impervious wall effectiveness becomes

$$\eta = m_W / m_C$$

The use of mass concentration as the conserved property overcomes the problem of the non-adiabatic wall encountered where enthalpy is used as the conserved property. The wall, in this case, is virtually impervious, the only mass flow through the wall being that required for sampling and this is a very small quantity indeed.

The second drawback attributed above to the measurement of effectiveness based upon temperature is also present where mass conservation is employed and this may be more or less serious depending upon the choice of tracer gas and the equipment used to measure concentrations. For instance, it is desirable to use a tracer gas with properties similar to those of air but not itself present in room air. Further, the chosen gas must be readily detectable to a high precision. These requirements are very difficult to fulfil. Gases which are most readily detectable are those with densities greatly different from that of air such as hydrogen or helium but these must be used with very small concentrations to avoid density gradients and, as the concentration diminishes, so does the precision of its measurement.

New problems also arise in using mass concentrations; e.g., the value of wall concentration is obtained by analysing a sample of air which is sucked through a sampling hole in the base plate of the wind tunnel. To what extent is the concentration of the tracer gas in this sample affected by the rate of suction? It was, however, considered possible that the advantages of measuring mass concentrations would outweigh the disadvantages and most of the remainder of this report

is concerned with providing answers to questions of the type posed above and to describing the method which was used to obtain the impervious wall effectiveness measurements reported in Table 4.

5.1 Chromatographic equipment

A Shandon KG-2 Chromatograph was selected to measure the concentration of the tracer gas in air. Preliminary tests indicated that a stainless steel column, 4 mm bore, 2 metres long and packed with Linde type Molecular Sieve was suitable for separating helium or hydrogen from air. Some difficulty was experienced in separating argon from air. The same equipment with a stainless steel column, 4 mm bore, 75 cm long and packed with Silica Gel satisfactorily separated carbon dioxide from air.

The thermal conductivity cell, which is an integral part of the Chromatograph, permitted very low concentrations of helium in air to be detected to a high precision. For example, 0.5% by volume of Helium in air can be detected to approximately 1% of the 0.5%. This together with the fact that the concentration of helium in air is very low, i.e., less than 30 ppm, and the experience gained in conducting preliminary tests suggested the use of helium as the tracer gas with slot concentrations of the order of 0.5 to 1.0% by volume.

Further tests indicated that either nitrogen or argon would be a suitable carrier gas. In either case, the helium passed through the detector in approximately 30 seconds, followed by oxygen approximately 90 seconds later. For the range of concentrations between 0.5 and 1% (by volume), the helium and oxygen peaks, as indicated by a potentiometer recorder, were of approximately the same height and since the oxygen peak is not sensitive to changes in concentration of the order of 1% of the tracer gas i.e., 0.01% of oxygen, but is sensitive to changes of the order of 1% of the oxygen, the oxygen peak provided a running check on the quantity of gas injected into the chromatograph. This proved to be of importance since syringe injection was latterly preferred to injection by means of an injection valve. In fact the effectiveness at any downstream position, x, was calculated by taking the ratio of helium to oxygen peak at the value of x, divided by the ratio of helium to oxygen at the slot. It should be noted that although previously effectiveness was discussed in terms of mass concentration and it is now found that the chromatograph indicates a concentration based upon thermal conductivities, the difference is of no consequence since the calculation of effectiveness uses a ratio of two concentration values based upon the same property. Provided the relationship between mass concentration, or volume concentration, and concentration based upon thermal conductivity values is a linear one, this procedure is justified.

Thus it is proved desirable to calibrate the chromatograph in the region of concentrations which was intended for use. This calibration was carried out by injecting known amounts of helium into a bottle of known (approximately) volume, stirring the mixture with a magnetic stirrer and injecting 1 ml of the mixture into the chromatograph. This injection was repeated several times to ensure reproducibility.

The/

The whole process was then repeated with a variety of concentrations and the resulting curve of the ratio of helium to oxygen peak heights against the volume of helium in the bottle, is presented in figure 14. It may be seen from this figure that in the peak height ratios range from 0.5 to 1.5. These data may be represented by a straight line. The maximum deviation from this line is of the order of 2% and these points are the average of many readings where scatter at any one value of the ratio of peak heights did not exceed 6%.

The measurements shown in figures 12-19 were almost all obtained with peak height ratios in the range 0.5 to 1.5. A very few points, were obtained with peak height ratios as low as 0.3 and these were at the furthest downstream locations.

5.2 Sampling method

A variety of methods were tried in order to obtain samples of the helium air mixture at the wall. In all of these the 0.020" holes drilled in the base plate of the wind tunnel were used, the samples being obtained by sucking through certain of these holes.

Having selected helium as the tracer gas it was not economically possible to have it flowing for a lengthy period of time. Consequently continuous flow measurements were ruled out and a method had to be found of obtaining samples in a short time (say 3 or 4 minutes) and measuring their concentration after the tracer gas had been shut off. The apparatus designed for this purpose is shown in figure 15. It consists of a series of 15 bottles of 20 ml capacity with a glass valve at the bottom end. The bottom stem of each bottle is sealed into a large vessel and projects downwards into a pool of high vacuum oil. The upper stem is corrected through a piece of thick wall rubber tubing to an additional valve and thence, by means of small bore pvc tubing, to the selected holes in the base plate of the wind tunnel.

To measure the effectiveness of a particular jet configuration, the two fans are switched on and the velocities adjusted to the selected values. The two valves on each sampling bottle are opened and air pressure is applied through the 'T' piece provided until the oil level in each bottle is close to the upper valve. The upper valves are then closed, the pressure connection closed off and the vacuum connection opened. The vacuum pump is turned on. Helium is then added to the secondary air flow at inlet to the fan, the flow rate of helium being measured by a rotameter. The air and helium are allowed to flow for about 15 seconds and then the upper valves on all bottles are opened and the oil is sucked into the large glass vessel, flushing each bottle in the process. The air plus helium mixture is allowed to flow through each bottle for approximately 2 minutes and then both valves on each bottle are closed and the helium and vacuum pump are turned off. The mixture in each bottle is then ready for sampling. For all of the measurements recorded here, the sampling procedure began shortly after the helium flow had been shut off. Sampling was effected with the aid of 1 ml gas-tight syringe, samples being obtained by piercing the thick wall rubber tubing with the needle of the syringe. Samples obtained in this way were immediately injected into the chromatograph.

Two/

Two specific tests were carried out to check the precision of this method of sampling. The first investigated the possibility of leakage, by diffusion, from the sampling bottles and the second the effect of the rate of sampling upon the measured value of contraction.

In the first test it was found that there was no appreciable change in the concentration measured by the technique described above after a time of 24 hours, provided all the connections and stop cocks were properly greased and provided the injection needle was sharp. It was found to be good practice not to let the samples remain in the sample bottles for longer than necessary and, preferably, for less than one hour. It was also found desirable, if a 1 ml sample was removed from a particular sample bottle and another was required from the same bottle at some later time, to smear the hole in the rubber tubing, caused by the injection, with high vacuum grease.

The test of the effect of sampling rate was carried out in a very simple manner. The rate of flow of the sample was controlled by inserting a length of capillary tubing between the glass vessel containing the high vacuum oil and the vacuum pump. A sampling rate of approximately 1 ml/s was selected and a set of samples obtained for a particular setting of the secondary and main stream velocities. This test was repeated with flow rates of approximately 5 ml/s and 0.2 ml/s. The helium concentrations of the various samples were determined as indicated and the resulting values of the impervious wall effectiveness were significantly the same for the three sampling flow rates at any particular downstream position. It was concluded that providing the sampling rate was maintained within these limits it should have no effect on the resulting value of effectiveness.

5.3 Two-dimensionality of the tracer gas flow

One further question remained to be answered before effectiveness measurement by the method indicated above could be considered satisfactory. Was the flow of helium two-dimensional at exit from the slot and at downstream positions?

Tests of the two-dimensionality of the flow of the helium tracer gas at the slot were carried out by sampling the slot flow on the centre line and 3" on either side of the centre line. These samples were drawn through wall taps at a value of the dimensionless distance, x/y_C, of 4 and the resulting values of helium concentration were found to agree within $\pm$ 1.5%. This test was carried out on several occasions and the results were always within the 1.5% scatter band. The value of m for these tests was 2.26. Similar tests conducted at x/y_C of 12 and 28 yielded values of helium concentration within a scatter band of 1.5%.

Tests of two-dimensionality at downstream location were carried out in a similar manner to those indicated above. Figure 16 indicates the departures from two-dimensionality encountered with the slot used for Run numbers 1 and 2 and figure 17 those encountered with the slot used for Run numbers 3 to 5. The results shown on figure 16 suggested the need for better mixing of the secondary flow. Consequently rods and screens were inserted in the secondary flow plenum chamber and these were present for all subsequent measurements.

The/

The effect of these departures from two-dimensionality may be judged by reference to figure 18 which shows the measured value of effectiveness plotted against the parameter m for various values of x/y_C. These axes have been chosen because they give a reasonably clear view of the experimental reproducibility. The data shown were obtained using three slot heights (nominally the same), the first as shown in figure 16, the second as shown in figure 17 and the third of height 0.251" with a total variation of 0.011" across the centre 12", the centre 6" being constant to within 0.003". It may be seen from figure 18 that some of the effectiveness measurements for Run number 1, 2 and 4 have been duplicated. Initially effectiveness measurements were made for Runs 1 and 2 using the slot shown in figure 16 - several sets of measurements were made and these were averaged to account for one of the points shown for Runs 1 and 2 on each line of constant x/y_C. Similarly one of the points attributed to each of Runs 4 and 5 were obtained using the slot shown in figure 17. All other points were obtained using the slot shown in figure 17. All other points were obtained using the 0.251" slot. This serves to indicate that the results are reproducible to at worst 7% of the local value of effectiveness and that this discrepancy may be due in part to the departure from two-dimensional flow. This deviation is equivalent to 3% of the maximum value of effectiveness.

5.4 Present measurements

The results shown in figure 18 have been averaged and these average values of the impervious wall effectiveness are presented in Table 4 and graphed on more usual coordinates in figure 19. The data presented in Table 4, Run 10, were obtained without the usual accompanying hydrodynamic profiles. Hence it was not possible to obtain directly values of m and R_C. However, the maximum velocity at the slot and the free stream velocity were measured for this run and the appropriate values of m and R_C obtained from figure 20. This figure indicates the precision with which the parameters m and R_C were obtained, the maximum deviation from the smooth lines being approximately 4% in the case of m and 1.5% in the case of R_C.

The results shown on figures 18 and 19 exhibit the trends which should be exhibited. It appears from figure 18 that the maximum effectiveness at any particular downstream position is obtained with a value of m which is between 1 and 1.2. Under ideal circumstances, this maximum should be attained when m = 1 and it must be assumed that the present deviation from unity is caused by the particular velocity profiles at the slot and by the geometry of the slot.

It is unlikely that detailed comparisons of the measurements presented in figures 18 and 19 with those of other authors would be useful since it has already been shown [15] that such measurements tend to be specific to one apparatus. In addition, it is possible that the turbulent Lewis number is not unity in the present measurements so that direct comparisons are of limited value. However, it is desirable to indicate that the orders of magnitude of the present results are similar to those of other authors and, therefore, figure 19b presents the measurements for $m < 1$ together with the correlating equation suggested by Stollery and El-Ehwany [27].

i.e.,/

$$\text{i.e., } \eta = 3.09\,(x/my_c)^{-0.8}\,R_c^{\,0.2} \qquad \ldots \quad 5.1$$

evaluated for runs 7 and 9.
This equation was derived on the assumption that the flow is boundary layer like and that the boundary layer thickness, δ, is given by

$$\delta = 0.37x\,R_x^{-1/5} \qquad \ldots \quad 5.2$$

A seventh power velocity profile was also assumed. It may be seen from reference 27 that equation 5.1 predicts values of effectiveness which are approximately 30% low in most cases. This suggests that the effectiveness values obtained for runs 7 and 9 are of the correct order of magnitude.

5.5 The turbulent Lewis number

It has already been stated that the measurements of impervious wall effectiveness presented in this paper should be identical to measurements of adiabatic wall effectiveness provided the turbulent Lewis number is unity. The direct measurement of the turbulent Lewis number, however, is very difficult and subject to large inaccuracies. However, the measurements of Zakkay, Krause and Woo [28] suggest that, for mass concentrations of helium of the order used in the present measurements, the turbulent Lewis number is unity.

It is probable that the simplest check of the appropriate value of the turbulent Lewis number is to repeat some of the measurements using a different tracer gas and one which is likely to have a different turbulent Lewis number, say argon. It is intended to carry out this test in the near future although it should be remembered that for the purposes of the present investigation it is not of importance.

Acknowledgement

The author is indebted to Professor D. B. Spalding, to Mr. M. P. Escudier and to Mr. W. B. Nicoll for many helpful discussions. Mr. Escudier was of assistance with the turbulence measurements and with the writing of the computer program for data reduction and Mr. Nicoll with the measurements of effectiveness. The work was supported by the Ministry of Aviation (Contract PD/37/043) to whom grateful acknowledgement is made.

Notation/

Notation

		Defined by
$c_f/2$	dimensionless shear stress	$\tau/(\rho u_G)^2$
d	tip height of total-head probe	-
H_{12}	shape factor	δ_1/δ_2
H_{32}	shape factor	δ_3/δ_2
m	mass flow ratio	$\rho_C \bar{u}_C/\rho_G u_G$
R_1	Reynolds number based on displacement thickness	$\delta_1 u_G/\nu$
R_2	Reynolds number based on momentum thickness	$\delta_2 u_G/\nu$
R_3	Reynolds number based on kinetic-energy thickness	$\delta_3 u_G/\nu$
R_C	Reynolds number based on slot height	$\bar{u}_C y_C/\nu$
R_x	Reynolds number based on distance along the wall	$u_G x/\nu$
T	temperature	
u	velocity in the main-stream direction	
$\bar{u}_C$	mean velocity at the slot	
u^+	dimensionless velocity	$u/\sqrt{\tau/\rho}$
x	distance along the wall in the main-stream direction	
y	distance normal to the wall	
y^+	dimensionless distance normal to the wall	$y\frac{\sqrt{\tau/\rho}}{\nu}$
δ	boundary layer thickness	

δ_1	displacement thickness	$\int_o^{y_G}(1-u/u_G)dy$
δ_2	momentum thickness	$\int_o^{y_G}u/u_G(1-u/u_G)dy$
δ_3	kinetic-energy thickness	$\int_o^{y_G}(u/u_G)[1-(u/u_G)^2]dy$
η	effectiveness	$(\phi_W-\phi_G)/(\phi_C-\phi_C)$
ν	kinematic viscosity of fluid	
ρ	fluid density	
τ	wall shear stress	
ϕ	any conserved property	

Subscripts

C	refers to properties at the slot
G	refers to properties of the main-stream fluid
W	refers to properties at the wall.

References/

References

No.	Author(s)	Title, etc.
1	G. H. Halls.	Some problems associated with cooling gas turbine combustion chambers. Rolls Royce Ltd., Aero Engine Division. Reference TB/GAH 1/MB 28.11.63.
2	K. Wieghardt	Hot air discharge for de-icing. A.A.F. Translation No.F-TS-919-RE, 1946
3	J. Odgers and J. Winter	Unpublished Lucas Gas Turbine Equipment Ltd. Report.
4	S. D. Barnwell and J. Palmer	Second interim report on performance investigations into two-dimensional models of film cooling. Unpublished. Bristol Siddeley Engines Ltd. Report Combustion Department, Report No.PD1396, December, 1965.
5	R. B. Price	Summary of cooling tests carried out on a film-cooled parallel duct. Bristol Siddeley Engines Ltd., Advanced Propulsion Research Grants, Report No. A.P.5312, May, 1965.
6	E. R. G. Eckert and R. C. Birkebak	The effects of slot geometry on film cooling. pp. 150-163 in Heat Transfer and Thermodynamics Education. Ed. H. A. Johnson, McGraw-Hill (1964).
7	J. H. Chin, S. C. Skirvin, L. E. Hayes and F. Burggraf	Film cooling with multiple slots and louvers. J. Heat Transfer, Trans. A.S.M.E. 83 C (1961) 281-286.
8	J. P. Hartnett, R. C. Birkebak and E. R. G. Eckert	Velocity distribution, temperature distributions, effectiveness and heat transfer for air injected through a tangential slot into a turbulent boundary layer. J. Heat Transfer, Trans. A.S.M.E. 83 C (1961) 293-306.
9	R. A. Seban, H. W. Chan and S. Scesa	Heat Transfer to a turbulent boundary layer downstream of an injection slot. A.S.M.E. paper No.57-A-36.
10	S. S. Papell	Effect on gaseous film cooling of coolant injection through angled slots and normal holes. NASA TN D-299 (September, 1960).

11./

No.	Author(s)	Title, etc.
11	J. H. Chin, S. C. Skirvin, L. E. Hayes and A. Silver	Adiabatic wall temperature downstream of a single injection slot. A.S.M.E. Paper No.58-A-107.
12	S. S. Papell and A. M. Trout	Experimental investigation of air film cooling applied to an adiabatic wall by means of an axially discharging slot. NASA TN D-9 (August, 1959).
13	R. A. Seban	Heat transfer and effectiveness for a turbulent boundary layer with tangential fluid injection. J. Heat Transfer, Trans. A.S.M.E. 82 C (1960) 303-312.
14	A. E. Samuel and P. N. Joubert	Film cooling of an adiabatic flat plate in zero pressure gradient in the presence of a hot mainstream and cold tangential secondary injection. A.S.M.E. Paper No.64-WA/HT-48.
15	J. H. Whitelaw	The effect of the geometry of the injection region on wall cooling processes. Imperial College Report IC/HRJ/35, (June 1965): see also A.R.C.27 373 (November, 1965).
16	D. B. Spalding	A unified theory of friction, heat transfer and mass transfer in the turbulent boundary layer and wall jet. A.R.C. C.P.829 (March, 1964).
17	F. H. Clauser	Turbulent boundary layers in adverse pressure gradients. J. Aero. Sci. 21 (1954) 91.
18	H. Schlichting	Boundary layer theory. 4th Edition p.537. McGraw-Hill (1960).
19	A. A. Townsend	The structure of the turbulent boundary layer. Proceedings of the Cambridge Philosophical Society Vol.47 page 375, 1951.
20	P. Bradshaw and D. H. Ferriss	The response of a retarded equilibrium turbulent boundary layer to the sudden removal of pressure gradient. N.P.L. Aero. Report No.1145, A.R.C.26 758 (March 1965).
21	V. C. Patel	Calibration of the Preston Tube and limitations on its use in pressure gradients. J. Fluid Mech. 23 (1965) 185-208.

22 /

No.	Author(s)	Title, etc.
22	R. C. Dean	Jr. Aerodynamic Measurements. M.I.T. Gas Turbine Laboratory, 1963.
23	L. Landweber	The analysis of flat-plate boundary-layer data. 9th I.T.T.C. Paris. September, 1960, p.121.
24	M. P. Escudier, W. B. Nicoll, D. B. Spalding and J. H. Whitelaw	The decay of a velocity maximum in a turbulent boundary layer. To be published in Aero. Quart.
25	W. B. Nicoll	Unpublished data relating to the experiments reported in reference 26.
26	M. P. Escudier and W. B. Nicoll	The entrainment function in turbulent boundary layer and wall jet calculations. Imperial College Report TWF/R/1: to be published in J. Fluid Mech. 25 (1966) 337-366.
27	J. L. Stollery and A. A. M. El-Ehwany	A note on the use of a boundary-layer model for correlating film cooling data. Int. J. Heat Mass Transfer 8 (1965) 55-65.
28	V. Zakkay, E. Krause and S. D. L. Woo	Turbulent transport properties for axisymmetric heterogeneous mixing. A.I.A.A. Journal 2 (1964) 1939-1947.

Table 1/

Table 1 : Contraction profile

Distance upstream of working section inches	Half-width inches	Half-height inches
0	9.00	6.00
1.8	9.04	6.03
3.6	9.10	6.07
5.4	9.20	6.14
7.2	9.34	6.23
9.0	9.54	6.36
10.8	9.82	6.55
12.6	10.19	6.80
14.4	10.67	7.12
16.2	11.30	7.54
18.0	12.42	8.28
19.8	14.22	9.54
21.6	15.93	10.62
23.4	17.16	11.44
25.2	18.13	12.08
27.0	18.94	12.63
28.8	19.64	13.10
30.6	20.24	13.50
32.4	20.77	13.85
34.2	21.23	14.15
36.0	21.65	14.44
37.8	22.05	14.68
39.6	22.41	14.92
41.4	22.72	15.14
43.2	23.00	15.33
45.0	23.24	25.49
46.8	23.44	15.64
48.6	23.62	15.74
50.4	23.76	15.84
52.2	23.87	15.92
54.0	23.94	
55.8	23.99	
57.0 (4' - 9")	24.00	16.00

Table 2/

Table 2 : Results of hydrodynamic measurements effected with the injection slot shown in figure 4a.

$u_{C_{MAX}}/u_G$ = 1.40

y_C = 0.285 inches

x (ft)	x/y_C	u_G (ft/s)	R_x	R_1	R_2	R_3	H	H_3	$c_f/2$
0.912	34.6	87.55	530000	-1557	-1832	-3872	0.850	2.114	0.0036
1.42	53.5	87.33	819000	- 466	- 673	-1454	0.692	2.160	0.0030
1.83	77	88.7	1063000	1233	922	1682	1.337	1.823	0.00245
2.75	116	88.0	1581000	1863	1387	2507	1.343	1.807	0.00230
3.24	137	86.5	1701000	2618	1952	3507	1.342	1.797	0.00206
4.24	179	85.5	2198000	3002	2255	4054	1.331	1.798	0.00188
4.83	203	85.8	2510000	3653	2811	5102	1.300	1.815	0.00184

Table 3/

Table 3 : Hydrodynamic measurements obtained with the injection slot shown in figure 4b.

RUN 1 : $u_{C_{MAX}}/u_G = 2.66$

$m = 2.26$

$y_C = 0.248$ inches

$R_C = 1.95 \times 10^4$

x (ft)	x/y_C	u_G (ft/s)	R_x	R_1	R_2	R_3	H	H_3	$c_f/2$
0	0	68.1	0	-10869	-26365	-89990	0.412	3.413	
0.21	10.08	69.3	87880	-11663	-23679	-72651	0.493	3.068	0.0102
0.42	20.16	68.1	172900	-12431	-23164	-67059	0.537	2.895	0.0095
0.83	40.32	68.4	346200	-12743	-20464	-53771	0.623	2.628	0.0080
1.67	80.65	67.4	680600	-12101	-16874	-40506	0.717	2.401	0.0059
2.50	120.97	66.5	1010000	-12695	-16716	-38766	0.759	2.319	0.00490
3.33	161.29	66.8	1367000	-12838	-16261	-36837	0.789	2.265	0.00414
4.17	201.61	66.4	1696000	-11212	-13880	-30991	0.808	2.233	0.0036

RUN 2 : $u_{C_{MAX}}/u_G = 1.94$

$m = 1.65$

$y_C = 0.248$ inches

$R_C = 1.416 \times 10^4$

x (ft)	x/y_C	u_G (ft/s)	R_x	R_1	R_2	R_3	H	H_3	$c_f/2$
0	0	68.8	0	-5567	-10066	-28006	0.553	2.782	
0.21	10.08	69.2	87110	-5306	- 8227	-20960	0.645	2.548	0.0076
0.42	20.16	67.9	169000	-5393	- 7748	-18872	0.696	2.436	0.0069
0.83	40.32	67.7	337600						0.0052
1.67	80.65	67.3	667700	-3657	- 4373	- 9526	0.836	2.187	0.00385
2.50	120.97	67.3	1020000	-3162	- 3710	- 7974	0.852	2.149	0.00322
3.33	161.29	66.8	1348000	-2400	- 2858	- 6135	0.840	2.147	0.00284
4.17	201.61	66.9	1682000	-1426	- 2062	- 4476	0.691	2.171	0.00247

RUN 3/

RUN 3 : $u_{C_{MAX}}/u_G$ = 2.01

m = 1.75

y_C = 0.253 inches

R_C = 1.46×10^4

x (ft)	x/y_C	u_G (ft/s)	R_x	R_1	R_2	R_3	H	H_3	$c_f/2$
0	0	66.9	0	-6183	-11269	-31948	0.549	2.835	
0.21	9.88	67.9	86520	-6205	- 9920	-25835	0.626	2.604	0.0079
0.42	19.76	67.3	171700	-5921	- 8706	-21534	0.680	2.474	0.0073
0.83	39.53	67.5	343300	-4871	- 6368	-14646	0.765	2.300	0.0053
1.67	79.05	67.1	679500	-3649	- 4376	- 9539	0.834	2.180	0.00386
2.50	118.58	68.5	1037000	-2999	- 3521	- 7542	0.852	2.142	0.00310
3.33	158.10	68.2	1377000	-2090	- 2567	- 5531	0.814	2.155	0.00265
4.17	197.63	67.1	1595000	- 206	- 675	- 1663	0.305	0.464	0.00226

RUN 4 : $u_{C_{MAX}}/u_G$ = 1.48

m = 1.22

y_C = 0.253 inches

R_C = 1.054×10^4

x (ft)	x/y_C	u_G (ft/s)	R_x	R_1	R_2	R_3	H	H_3	$c_f/2$
0	0	67.7	0	-1899	-3112	- 7575	0.610	2.434	
0.21	9.88	67.8	86520	-1408	-1799	- 4006	0.783	2.227	0.0049
0.42	19.76	67.4	171400	-1461	-1777	- 3859	0.823	2.172	0.0045
0.83	39.53	68.0	345500	- 658	- 836	- 1795	0.786	2.146	0.0035
1.67	79.05	67.2	683000	- 246	27	- 76	8.965	-2.761	0.0026
2.50	118.58	68.3	1043000	1025	688	1164	1.490	2.691	0.0023
3.33	158.10	68.2	1379000	1892	1369	2399	1.382	1.752	0.0020
4.17	197.63	66.6	1684000	2710	2005	3553	1.352	1.772	0.00185

RUN 5/

RUN 5 : $u_{C_{MAX}}/u_G$ = 1.00

m = 0.855

y_C = 0.253 inches

R_C = 7.49×10^3

x (ft)	x/y_C	u_G (ft/s)	R_x	R_1	R_2	R_3	H	H_3	$c_f/2$
0	0	67.2	0	1250	897	1587	1,393	1.768	
0.21	9.88	67.6	86710	2191	1796	3318	1.220	1.847	
0.42	19.76	66.3	170300	2391	1916	3510	1.247	1.831	0.0023
0.83	39.53	66.8	341800	2752	2108	3802	1.305	1.804	0.00198
1.67	79.05	66.1	676000	3354	2519	4499	1.331	1.786	0.00176
2.50	118.58	68.2	1046000	3798	2912	5227	1.304	1.795	0.00174
3.33	158.10	69.6	1465000	4631	3480	6204	1.331	1.783	0.00164
4.17	197.63	67.2	1737000	4555	3399	6058	1.340	1.782	0.00165

RUN 6 : $u_{C_{MAX}}/u_G$ = 0.906

m = 0.753

y_C = 0.251 inches

R_C = 6.65×10^3

x (ft)	x/y_C	u_G (ft/s)	R_x	R_1	R_2	R_3	H	H_3	$c_f/2$
0	0	68	0	2197	1383	2381	1.588	1.721	
0.21	9.96	68.4	88460	2772	2121	3802	1.306	1.792	
0.42	19.92	67.4	173600	2909	2184	3890	1.332	1.782	
0.83	39.84	69.4	357300	2994	2262	4046	1.323	1.788	0.00183
1.67	79.68	67.4	691400	3639	2695	4784	1.350	1.775	0.00171
2.50	119.52	69.2	1064000	3895	3020	5444	1.290	1.803	0.00176
3.33	159.36	69.2	1419000	4167	3225	5810	1.292	1.802	0.00174
4.17	199.20	67.7	1737000	4316	3303	5935	1.307	1.797	0.00173

RUN 7/

RUN 7 : $u_{C_{MAX}}/u_G$ = 0.824

m = 0.691

y_C = 0.251 inches

R_C = 5.95×10^3

x (ft)	x/y_C	u_G (ft/s)	R_x	R_1	R_2	R_3	H	H_3	$c_f/2$
0	0	68.0	0	2679	1671	2804	1.603	1.678	
0.21	9.96	68.8	89570	3300	2398	4202	1.376	1.753	
0.42	19.92	67.5	174900	3318	2397	4203	1.384	1.753	0.00170
0.83	39.84	68.0	352800	3503	2541	4474	1.379	1.761	0.00165
1.67	79.68	67.5	689600	4022	2987	5300	1.346	1.774	0.00166
2.50	119.52	69.1	1058000	4032	3096	5564	1.302	1.797	0.00176
3.33	159.36	68.7	1401000	4222	3214	5794	1.314	1.803	0.00277
4.17	199.20	66.8	1704000	4479	3429	6166	1.306	1.798	0.00173

RUN 8 : $u_{C_{MAX}}/u_G$ = 0.968

m = 0.817

y_C = 0.251 inches

R_C = 6.96×10^3

x (ft)	x/y_C	u_G (ft/s)	R_x	R_1	R_2	R_3	H	H_3	$c_f/2$
0	0	67.7	0	1612	1081	1888	1.491	1.746	
0.21	9.96	68.6	87290	2197	1769	3245	1.242	1.834	
0.42	19.92	67.3	172600	2485	1960	3562	1.268	1.818	
0.83	39.84	67.7	346800	2845	2132	3820	1.335	1.792	0.00190
1.67	79.68	66.9	688800	3427	2543	4528	1.348	1.781	0.00176
2.50	119.52	68.9	1065000	3872	2965	5321	1.306	1.795	0.00175
3.33	159.36	68.7	1382000	4085	3121	5597	1.309	1.794	0.00173
4.17	199.2	67.3	1693000	4345	3275	5852	1.327	1.787	0.00170

Table 4/

Table 4 (continued)

RUN 7		RUN 8		RUN 9		RUN 10	
x/y_c	η	x/y_c	η	x/y_c	η	x/y_c	η
4	1.00	4	1.00	4	1.00	4	1.00
12	1.00	12	1.00	12	1.00	12	1.00
28	0.89	28	0.92	28	0.685	28	0.91
44	0.707	44	0.815	44	0.452	44	0.841
60	0.570	60	0.700	60	0.367	60	0.782
76	0.489	76	0.601	76	0.312	76	0.707
92	0.436	92	0.560	92	0.291	92	0.70
108	0.406	108	0.520	108	0.266	108	0.70
131	0.363	131	0.477	131	0.230	131	0.647
155	0.330	155	0.446	155	0.193	155	0.597
168	0.306	168	0.414	168	0.188	168	0.558
180	0.288	180	0.390	180	0.175	180	0.523
204	0.257	204	0.342	204	0.260	204	0.457

Table 4/

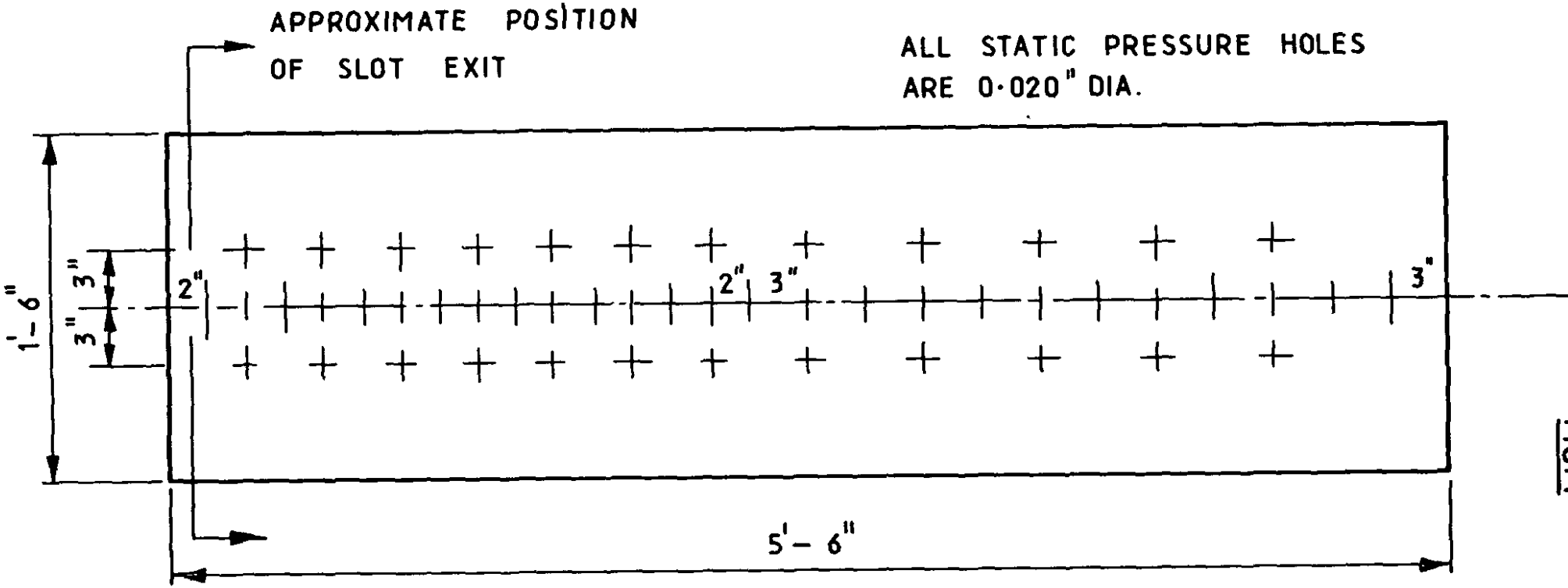

FIG. 1

Tunnel base plate showing location of static pressure holes

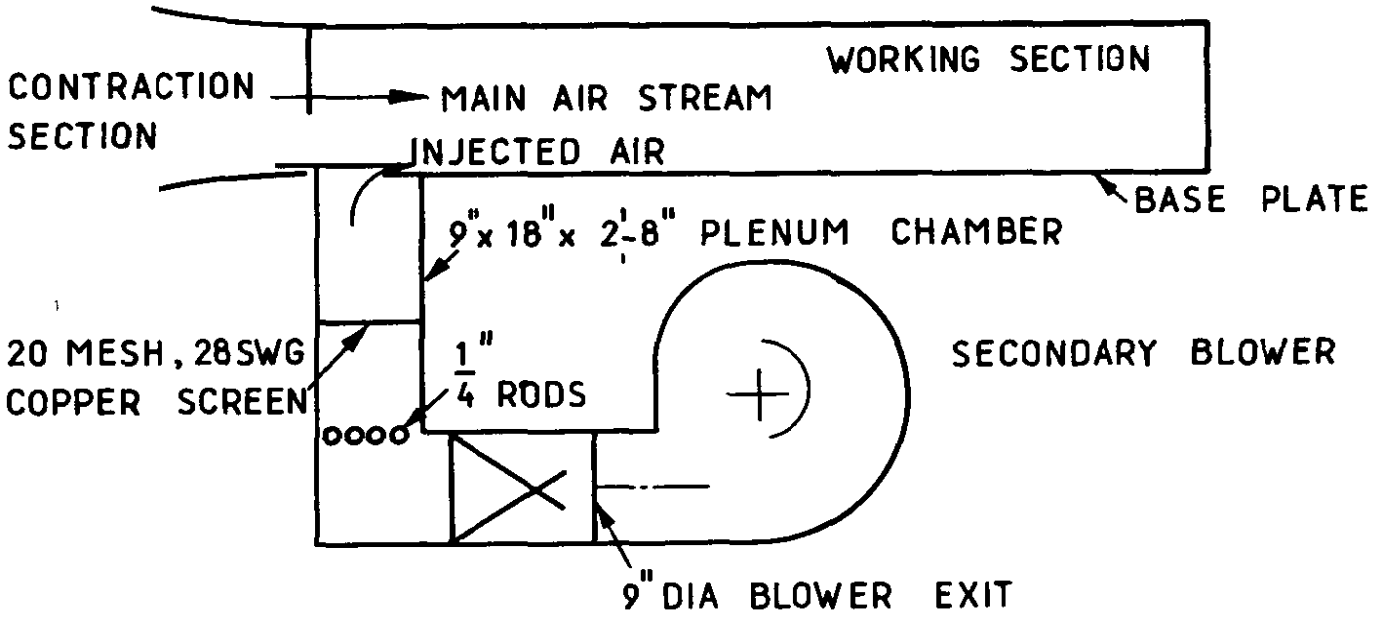

General arrangement of working section and secondary air system

FIG. 2

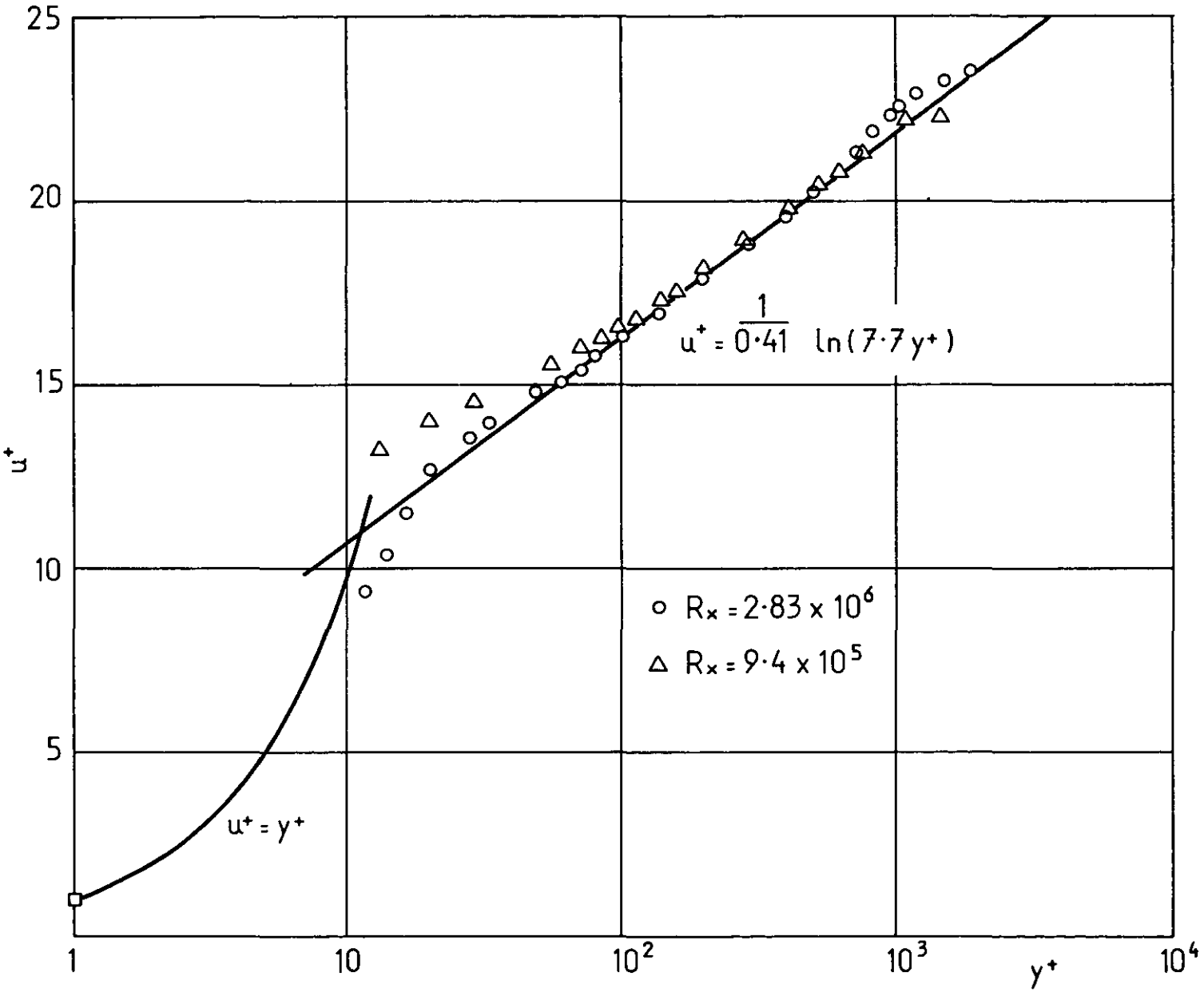

FIG. 3

Comparison of the universal velocity profile with velocity measurements obtained from flow on a flat plate

FIG. 4

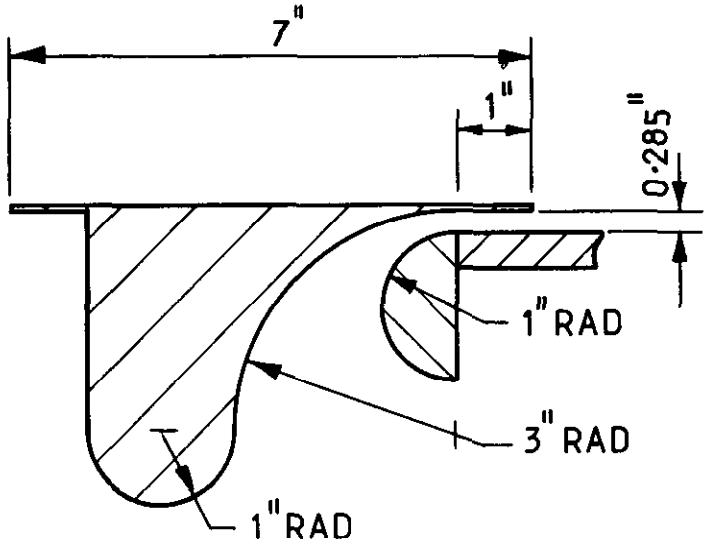

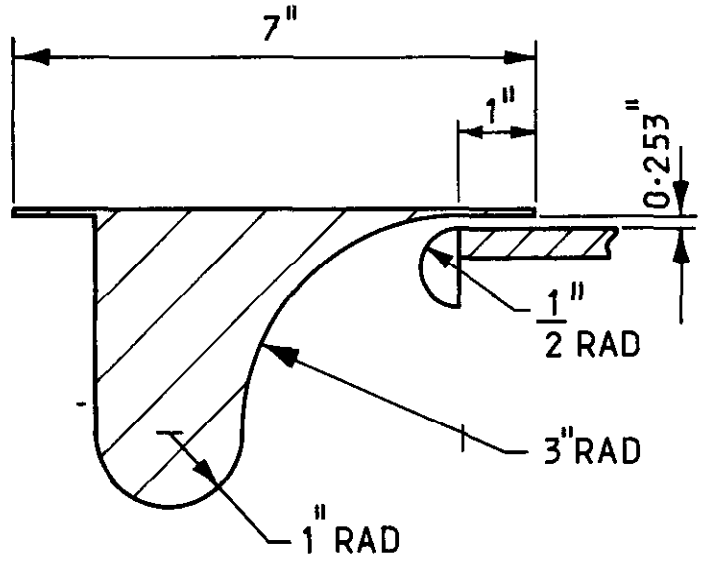

Slot configurations

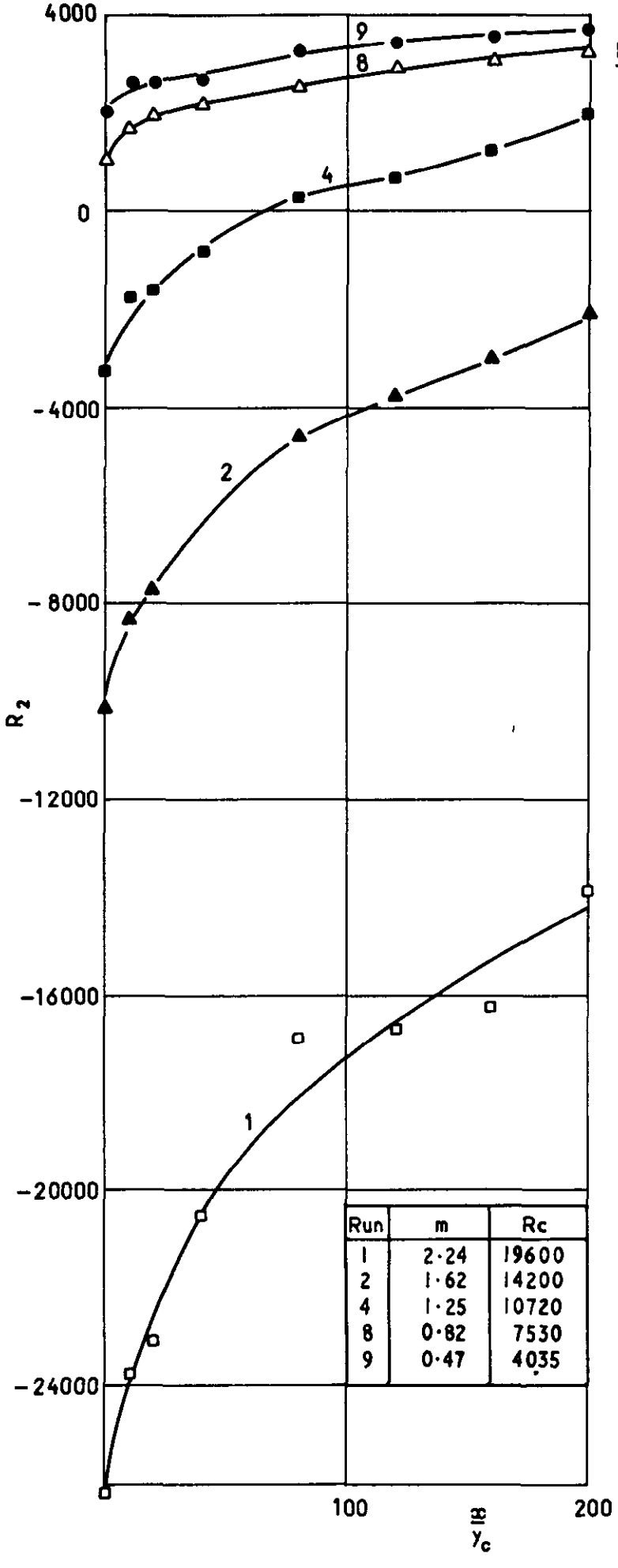

FIG. 5

The development of the Reynolds number, R_2 with downstream location

FIG. 6

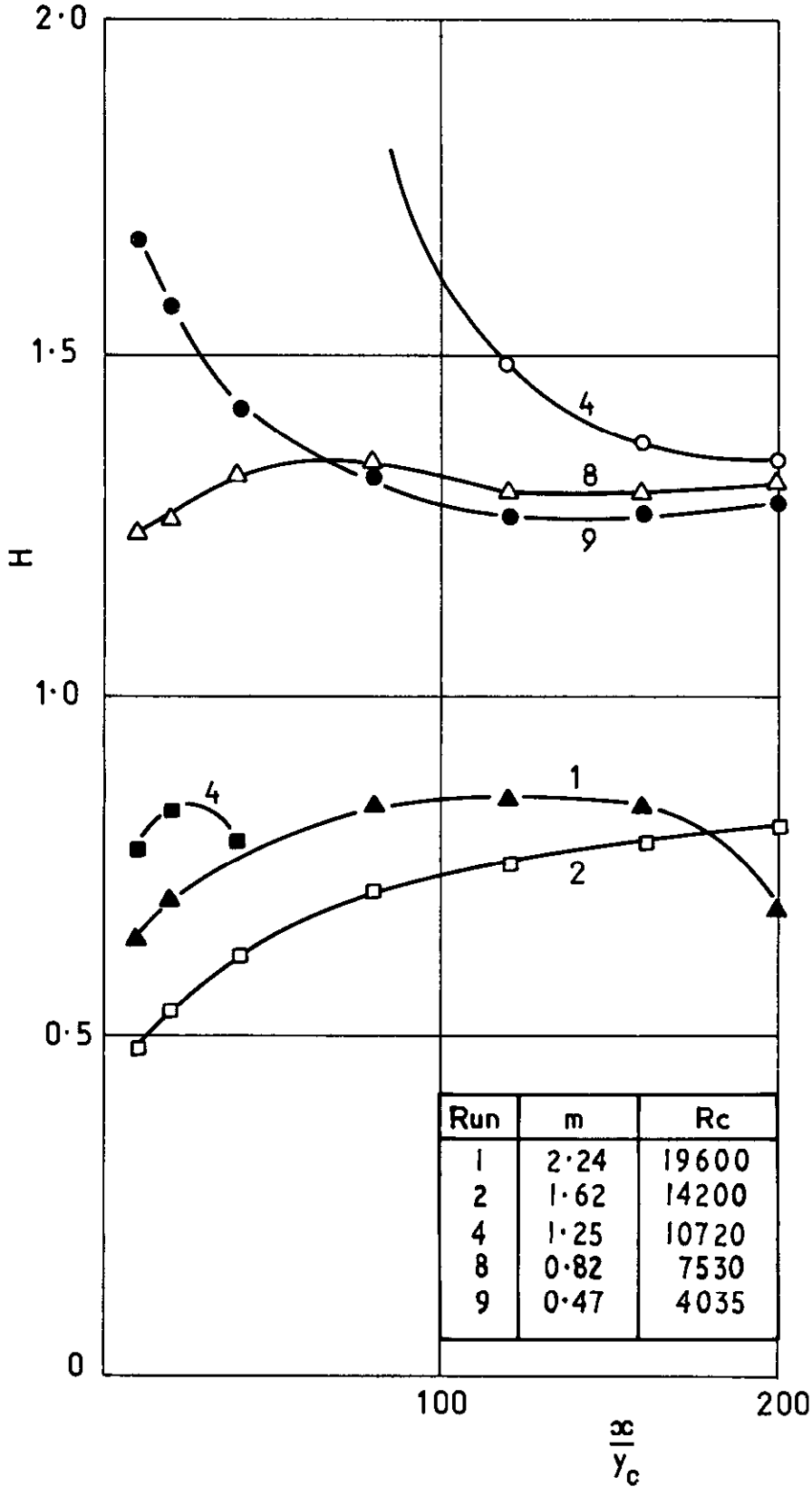

The development of the shape factor, H, with downstream location

FIG. 7

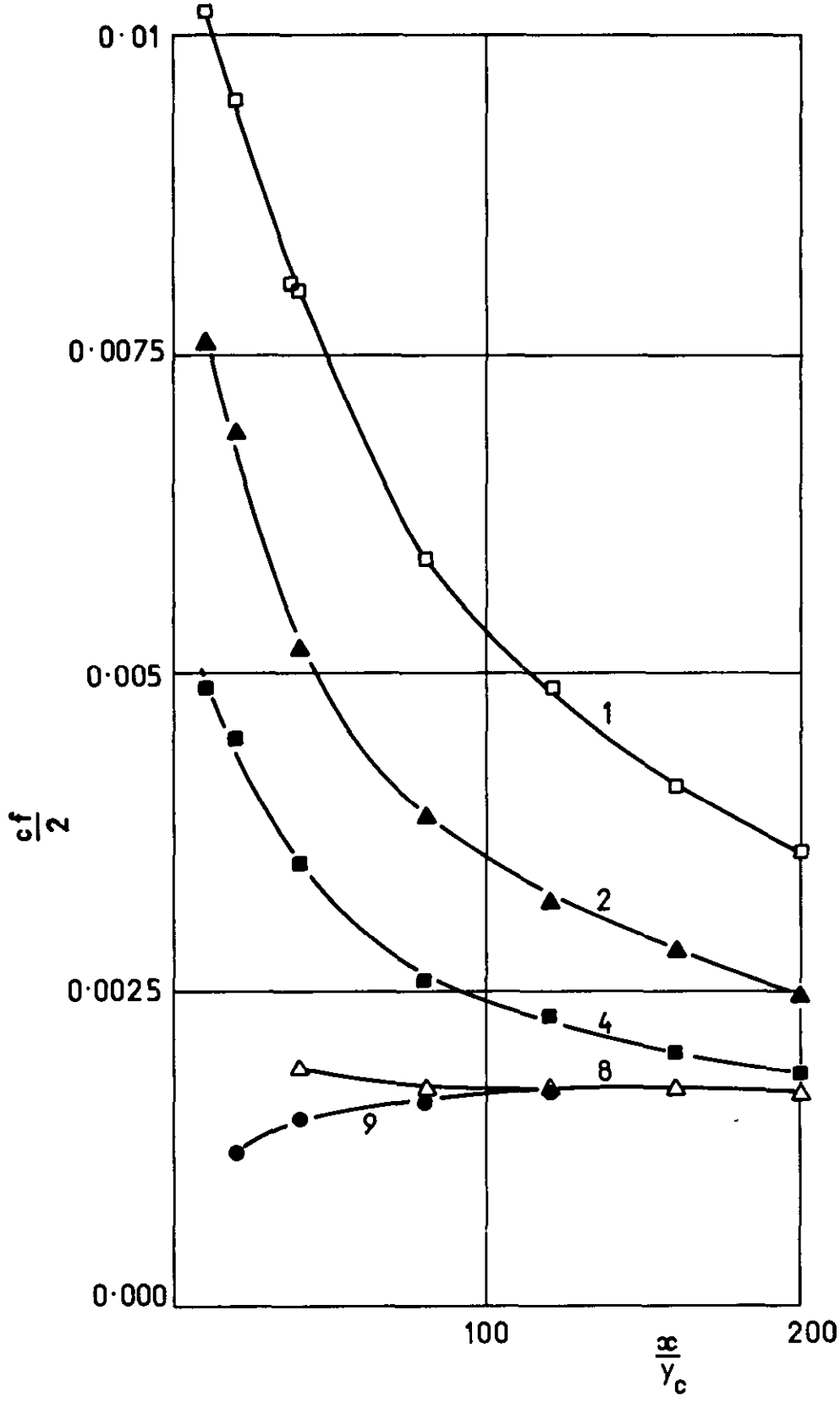

The development of the dimensionless shear stress, cf/2 with downstream location

FIG. 8

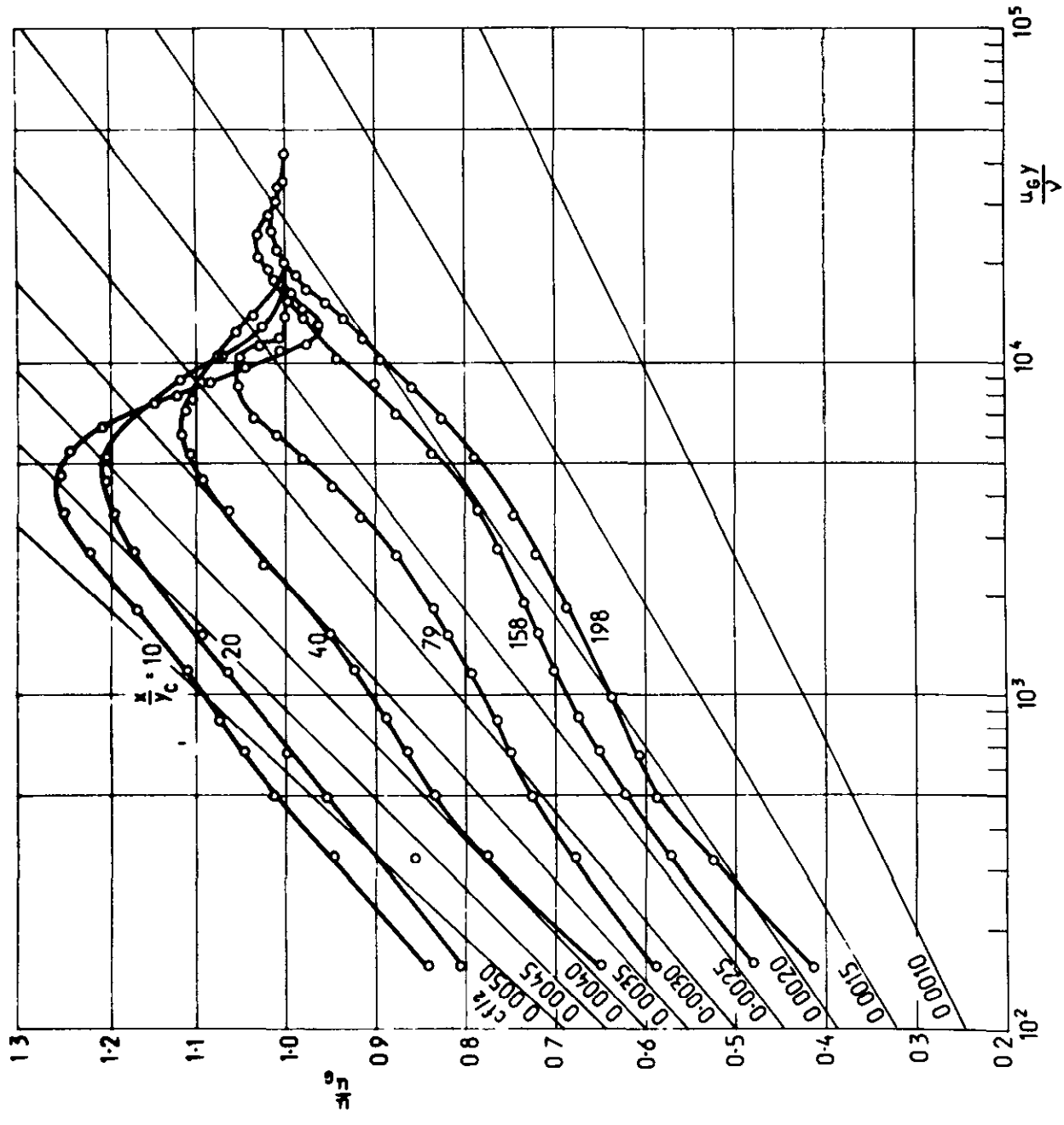

FIG 8 VELOCITY PROFILES FOR RUN NUMBER 4 LINES OF CONSTANT SHEAR STRESS WERE OBTAINED WITH THE AID OF EQUATION 51

FIG. 9

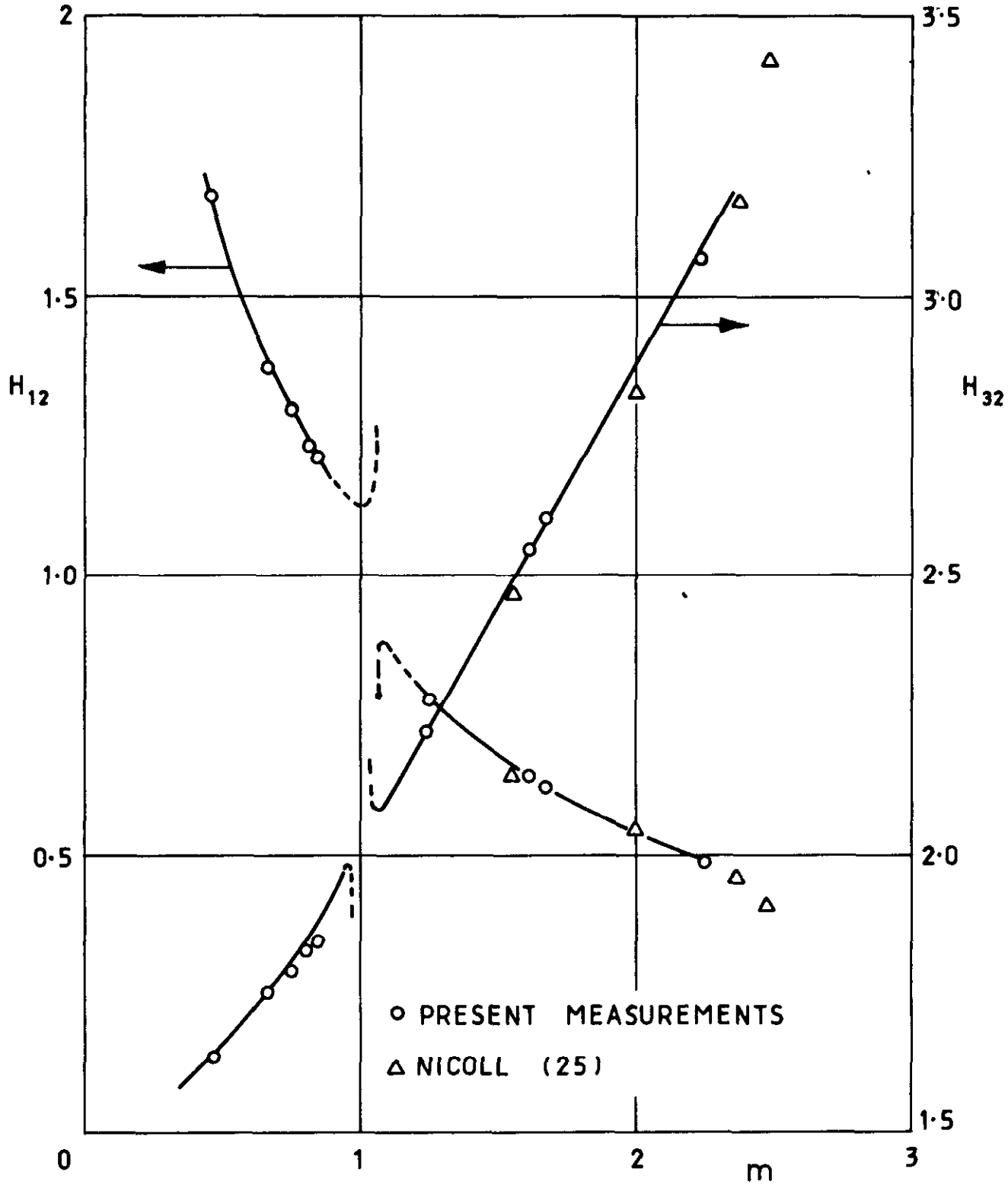

Starting values of the shape factors H_{12} and H_{32}, based upon slot conditions

FIG. 10

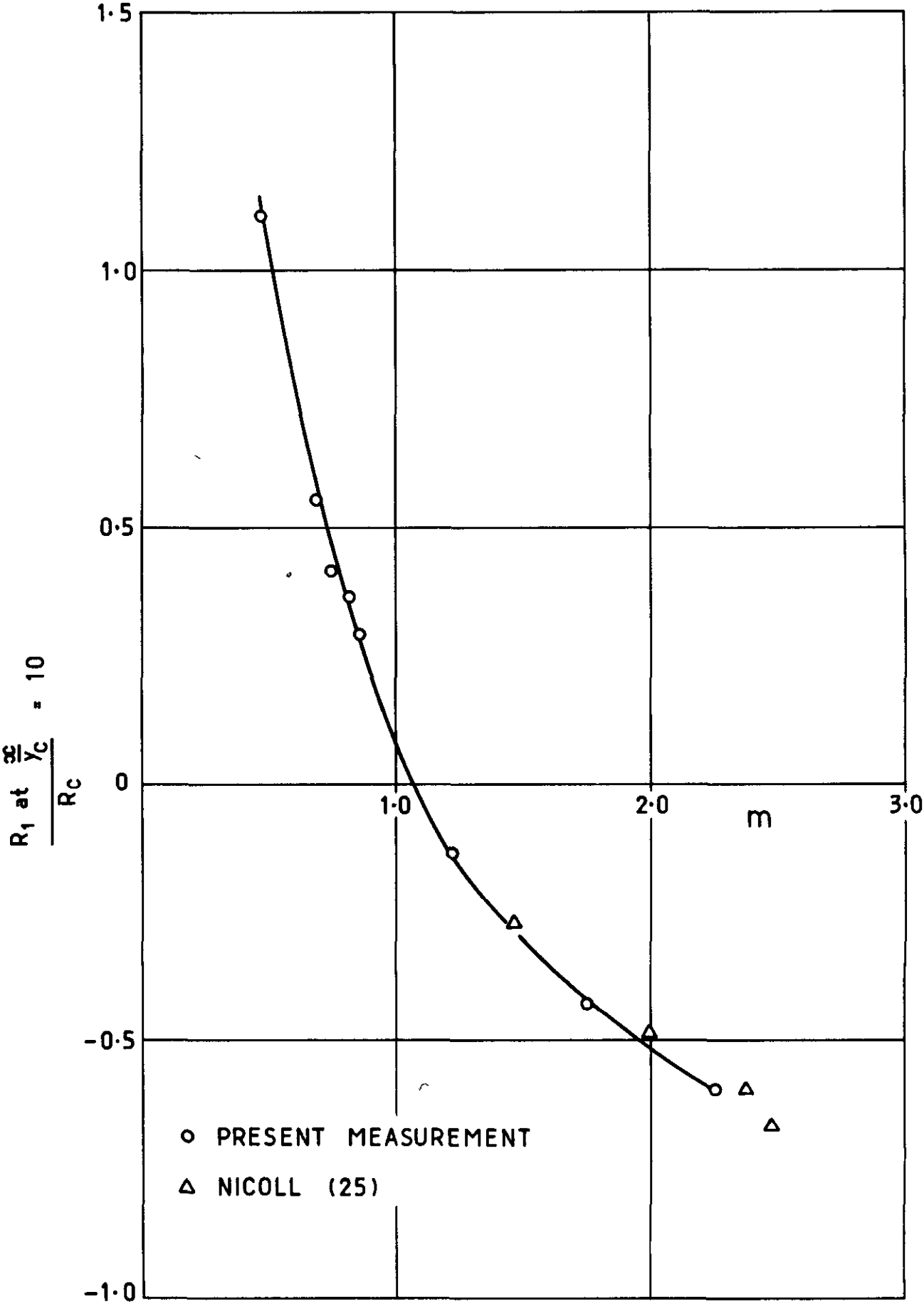

Starting values of the Reynolds number, R_1, based upon slot conditions

FIG. 11

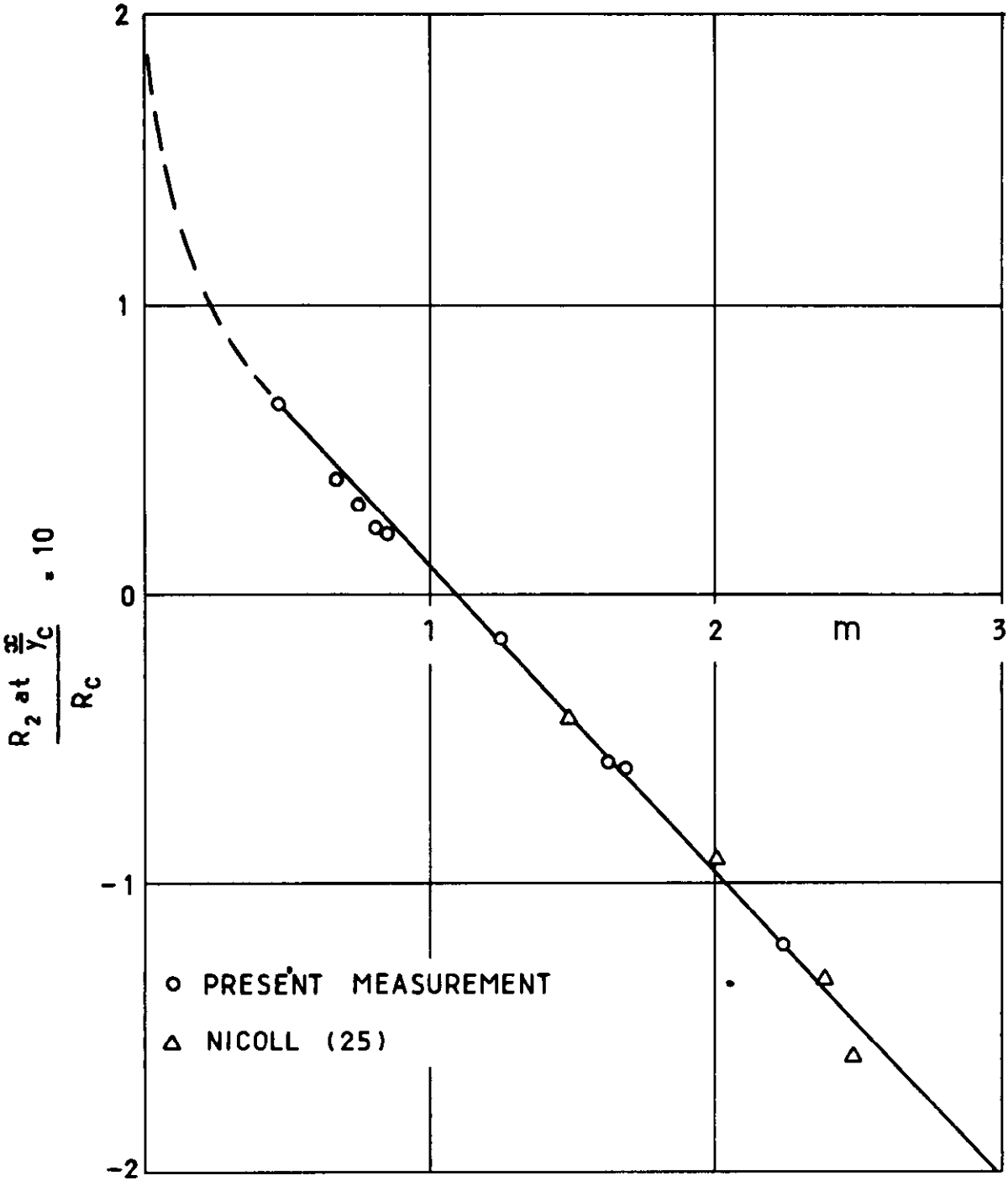

Starting values of the Reynolds number, R_2, based upon slot conditions

FIG. 12

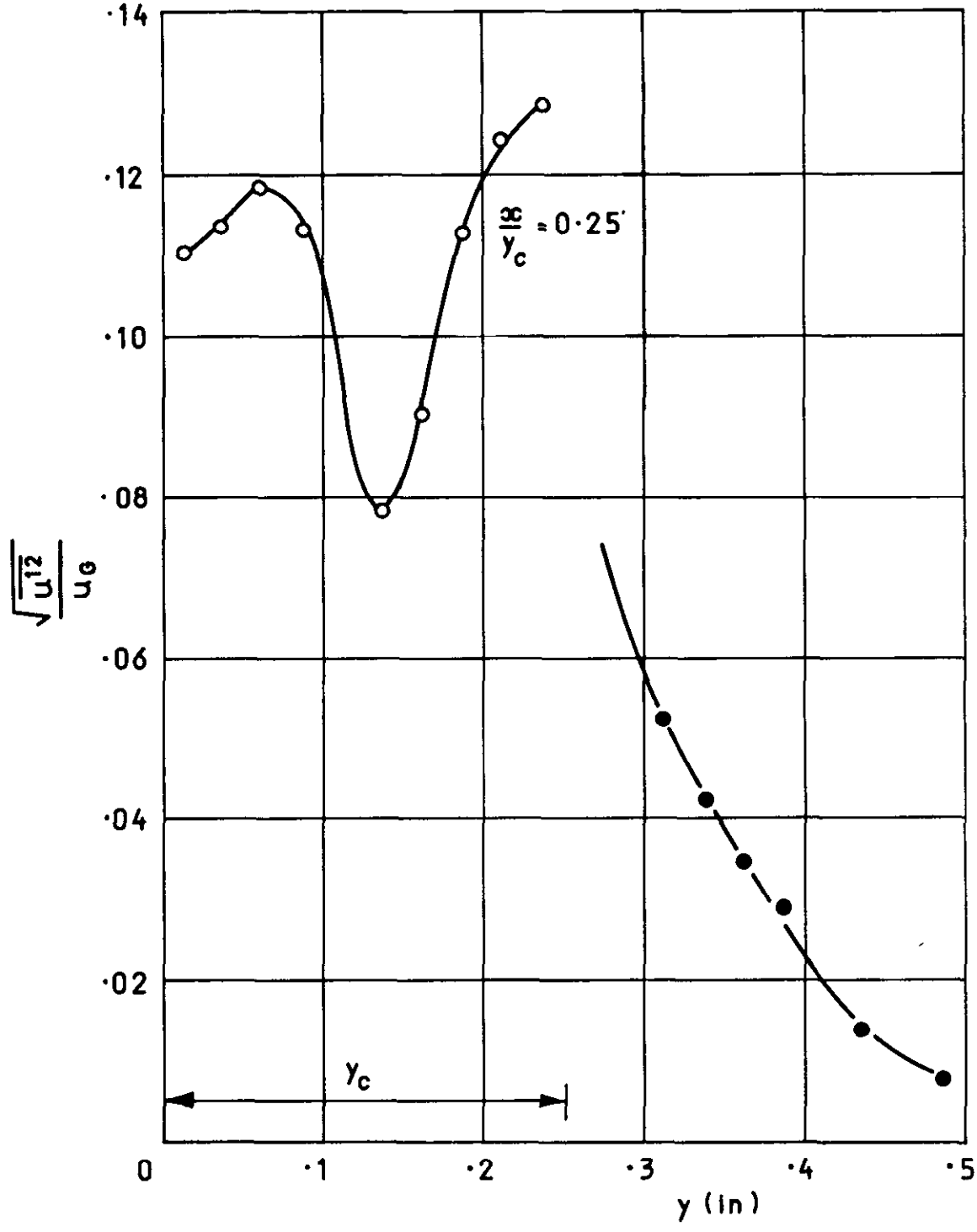

Turbulence – intensity profiles for $m = 1.62$

FIG. 13

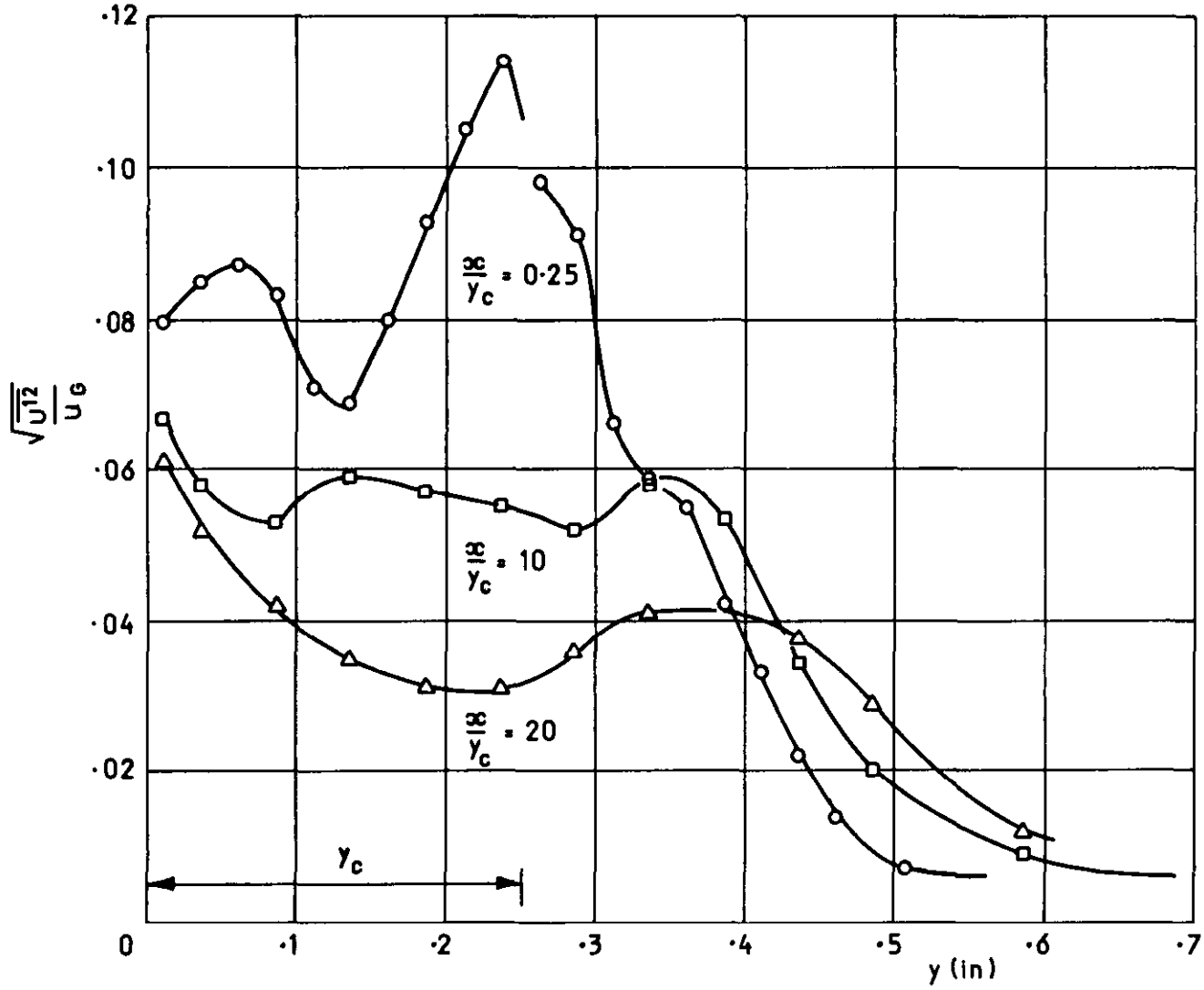

Turbulence – intensity profiles for m = 0·82

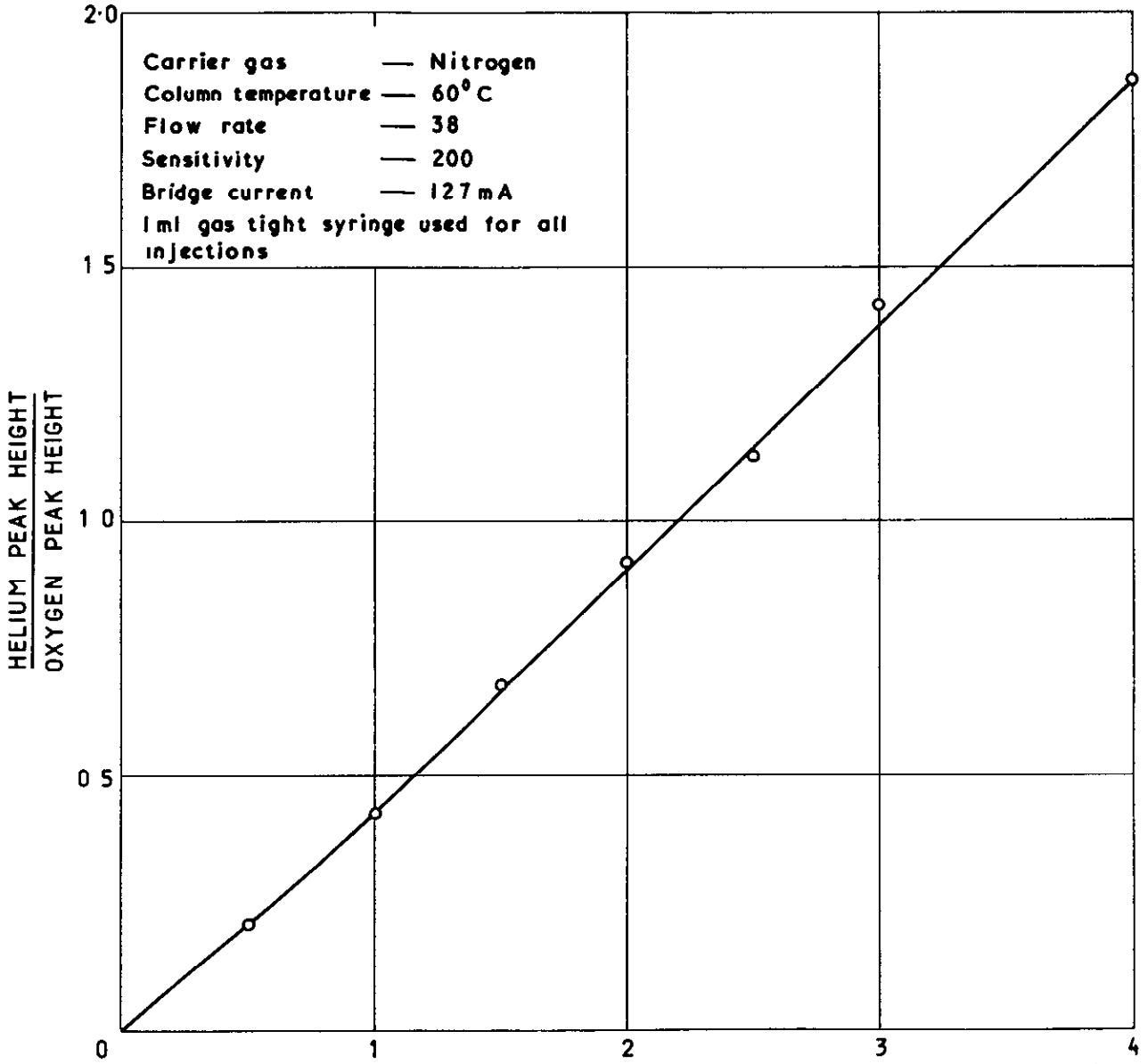

Calibration of the chromatograph

FIG. 14

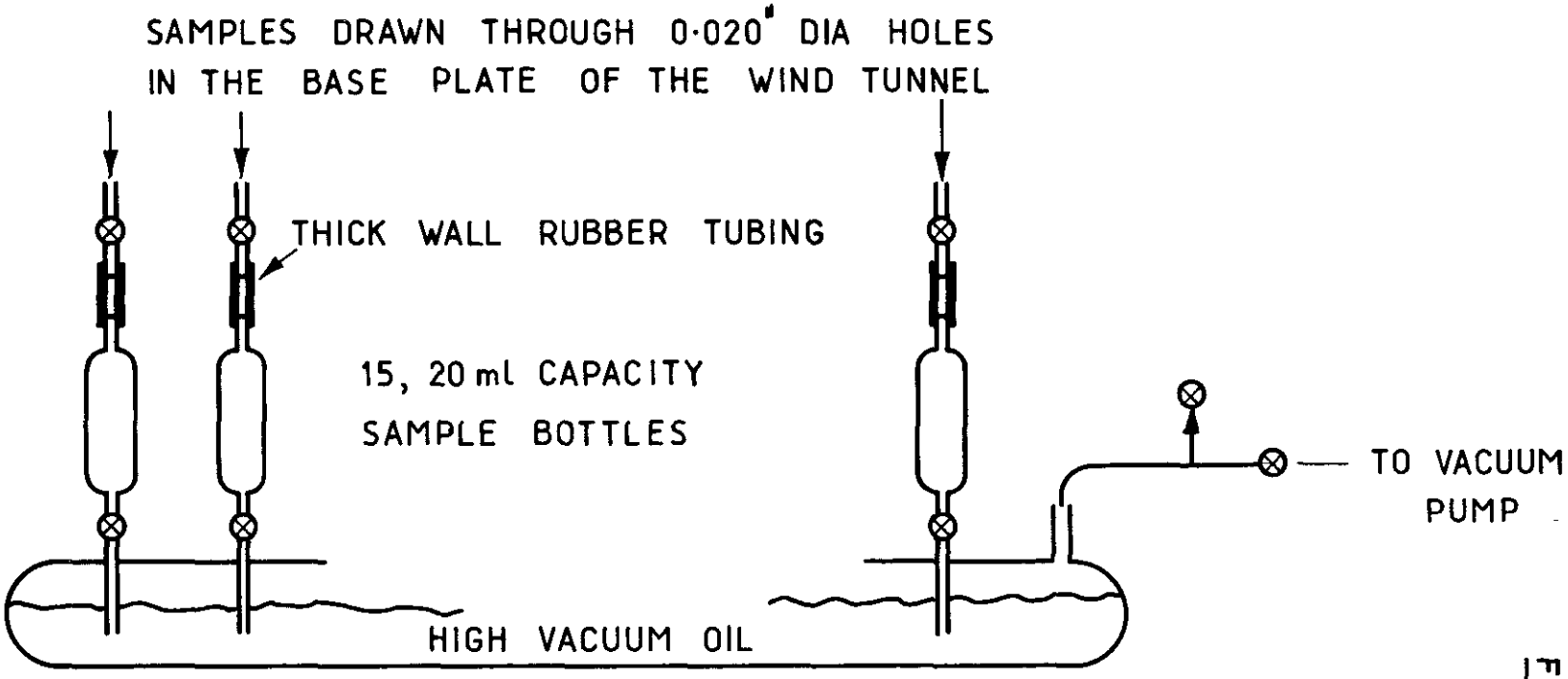

FIG. 15

Sampling system

FIG. 16

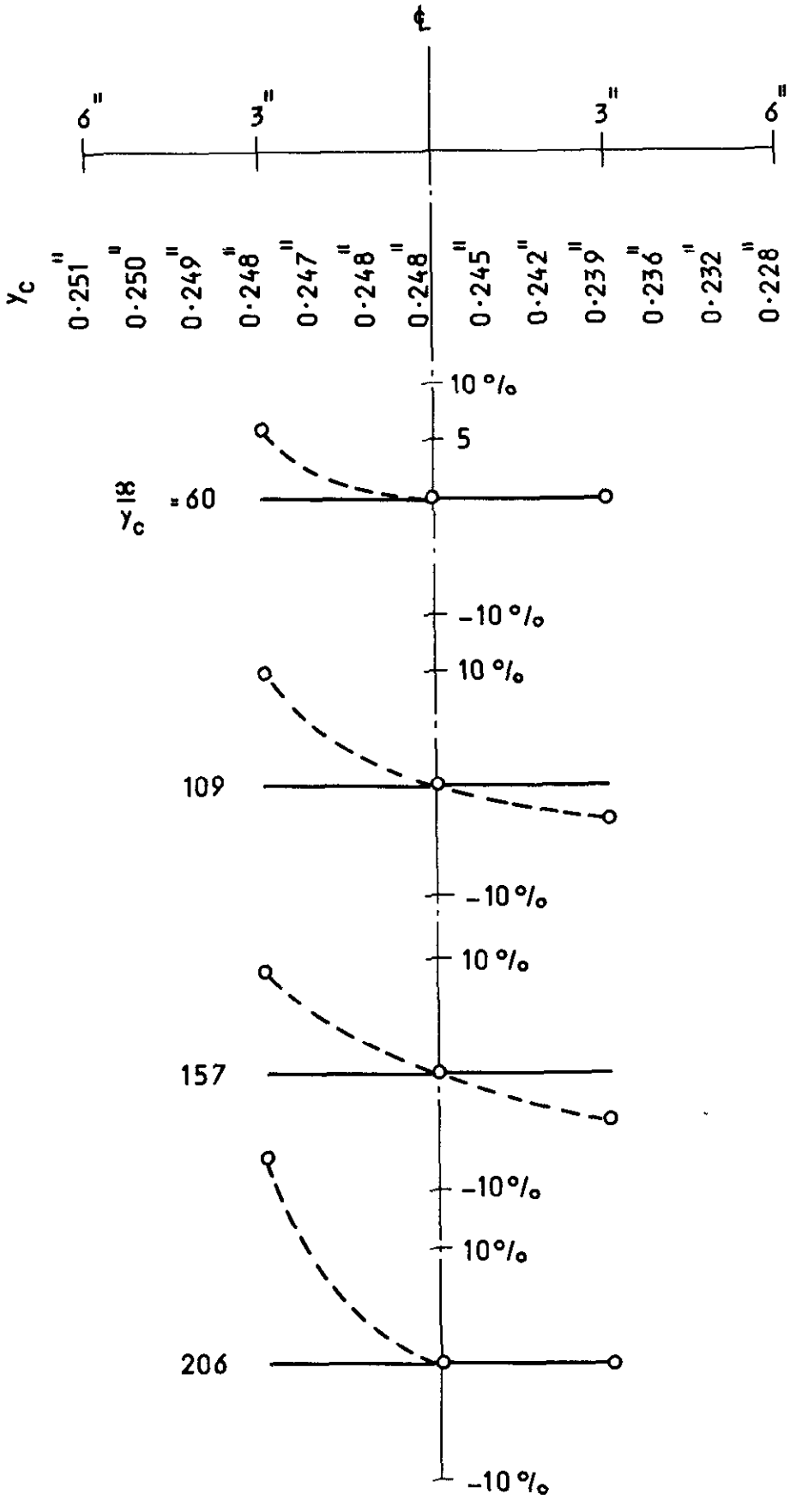

Percentage deviation of the local values of effectiveness from the centre line values at various downstream locations. M = 1·62

FIG. 17

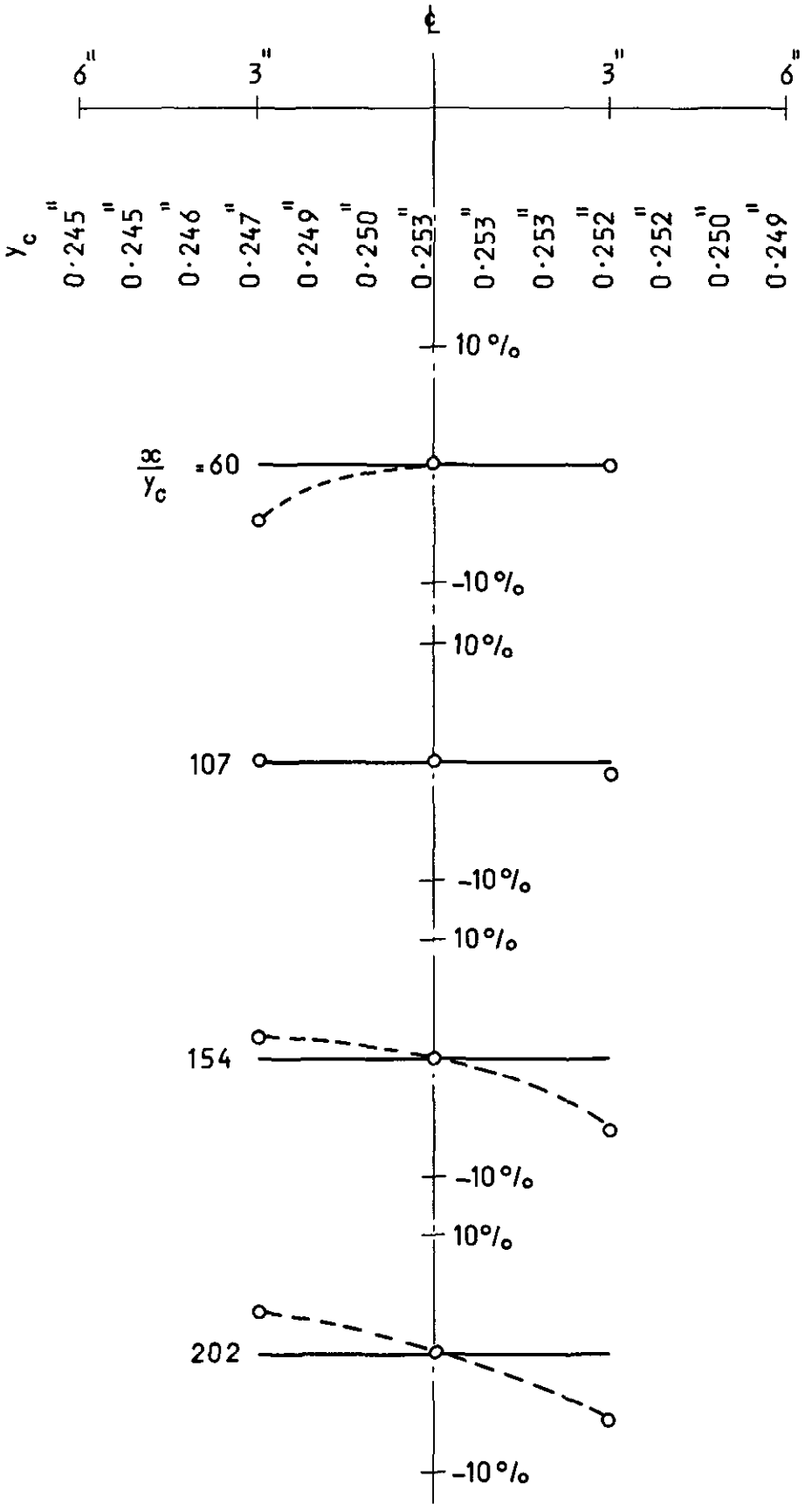

Percentage deviation of the local values of effectiveness from the centre line values at various downstream locations. $M \simeq 1 \cdot 68$

FIG. 18

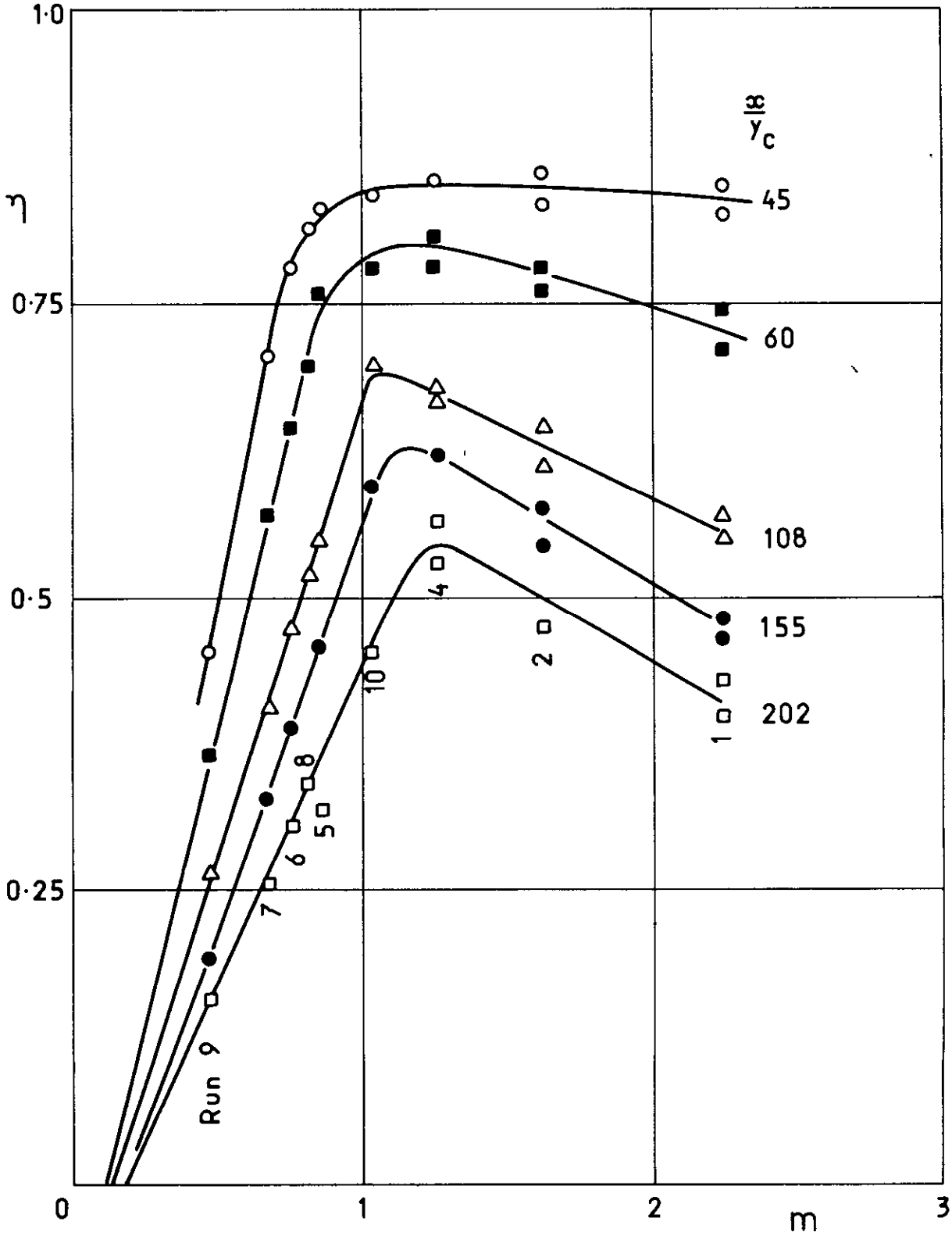

The impervious wall effectiveness at various downstream locations

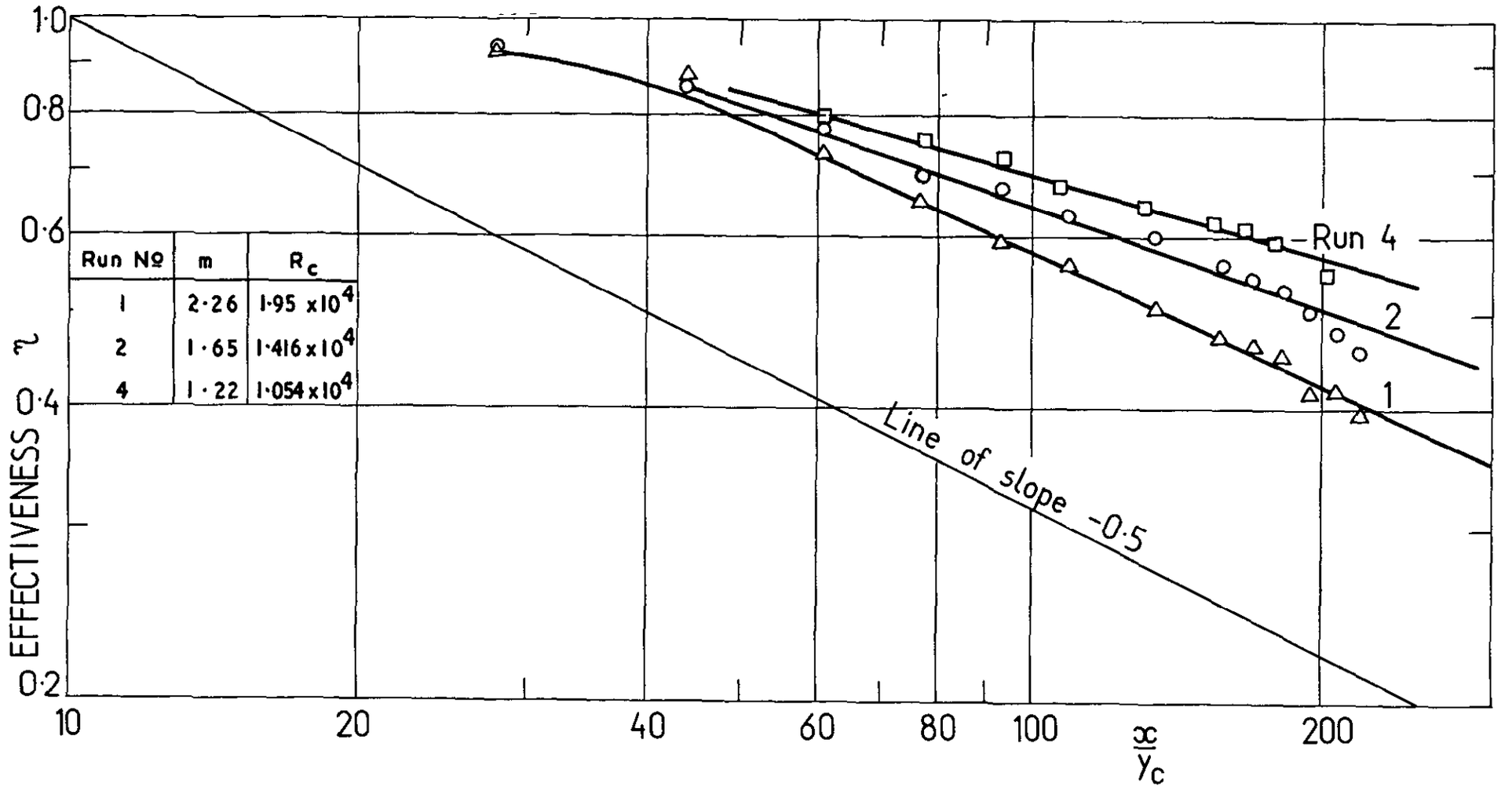

FIG. 19a

Impervious wall effectiveness obtained from concentration measurements of Runs 1, 2 & 4

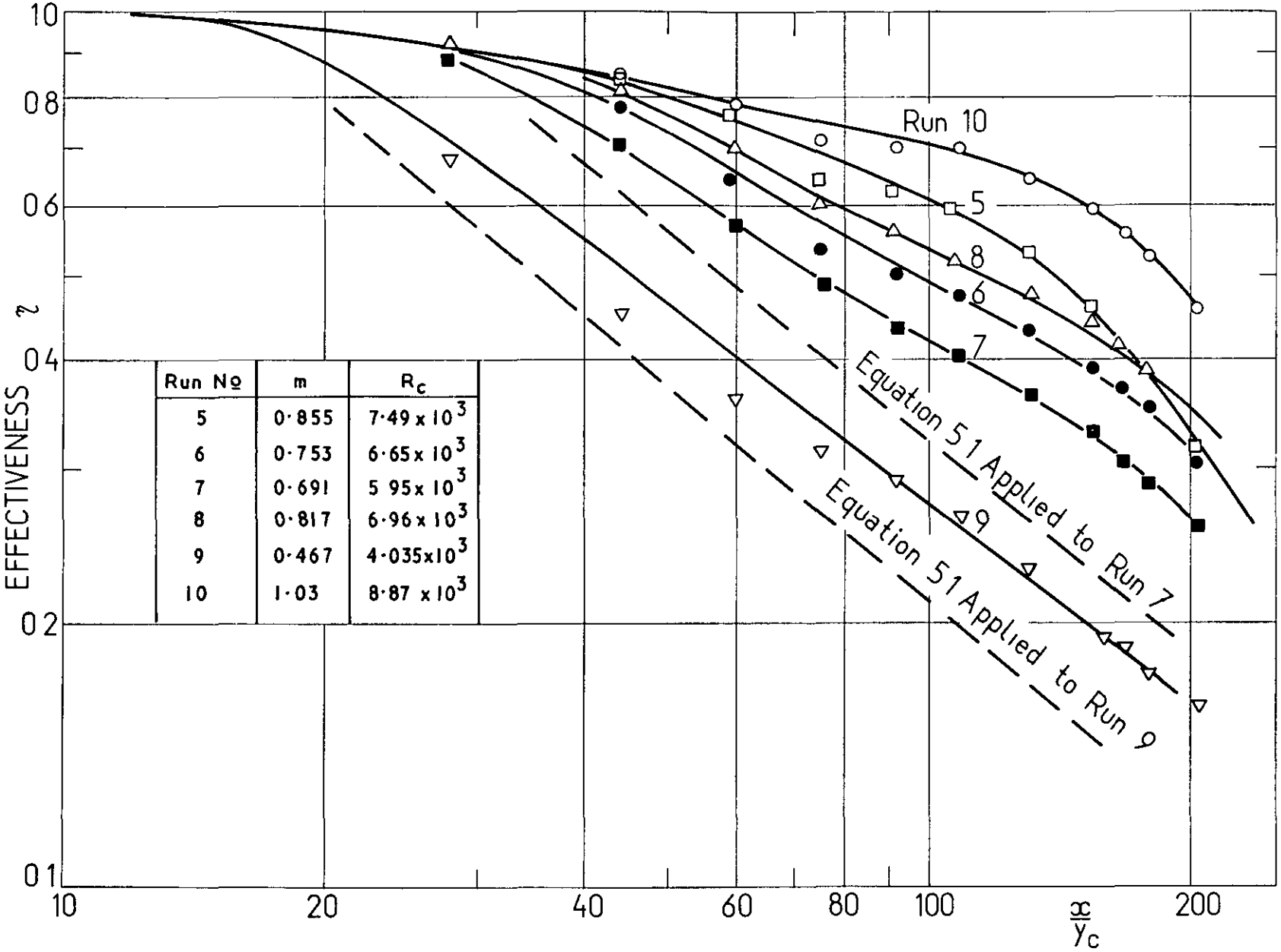

FIG. 19b

Impervious wall effectiveness obtained from concentration measurements of Runs 5–10

FIG. 20

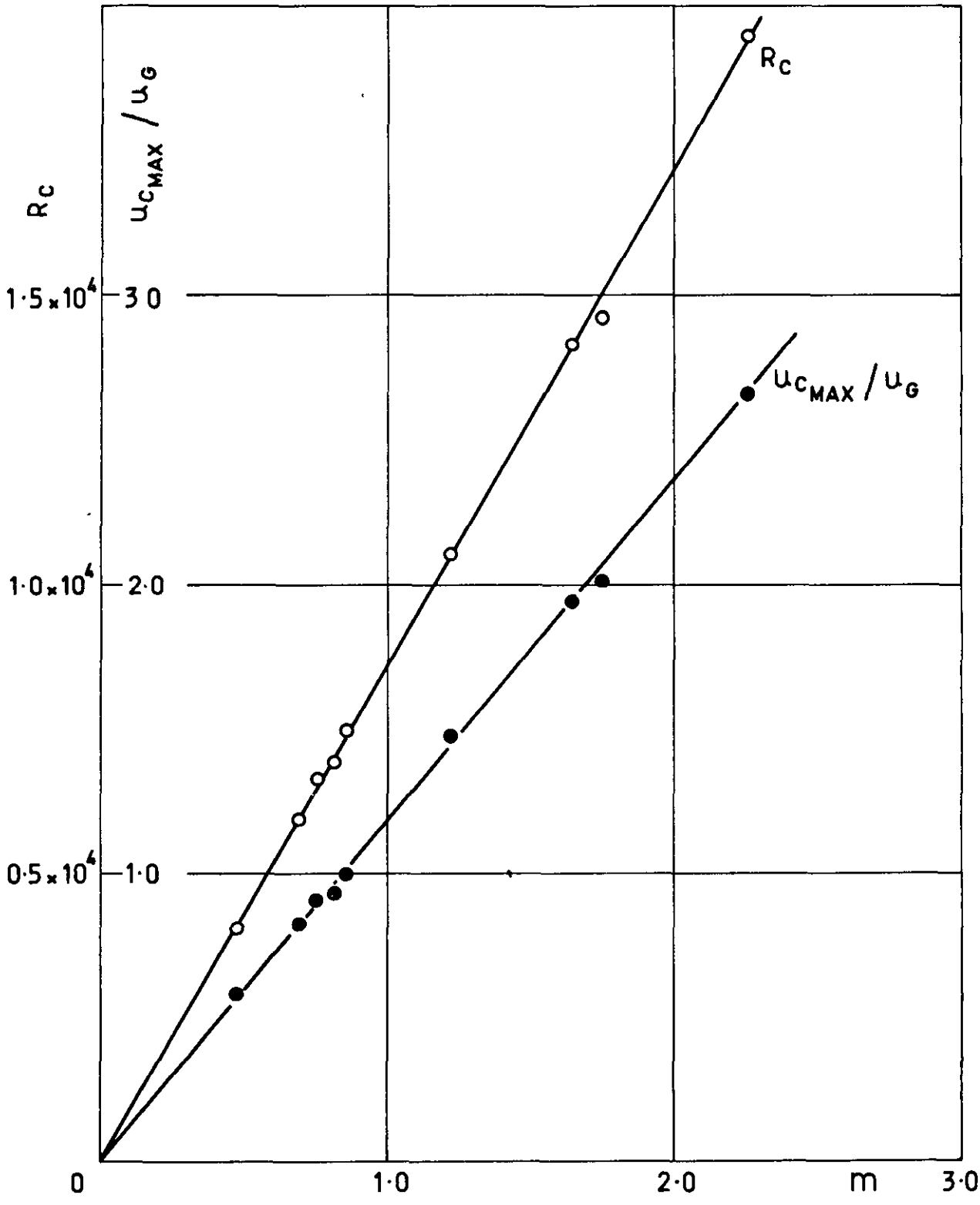

The relationships between R_C, $u_{C\,max} / u_G$ and the parameter m

A.R.C. C.P.942
April, 1966
J. H. Whitelaw

AN EXPERIMENTAL INVESTIGATION OF THE TWO-DIMENSIONAL WALL JET

A new apparatus, designed to investigate the effects of slot geometry on the effectiveness of film cooling, is described and new measurements of the impervious wall effectiveness are presented. The measurements were performed in the range $2.24 \leq m \leq 0.47$ using helium as a tracer gas and gas chromatographic equipment to detect the relevant concentrations. The appropriate hydrodynamic quantities are reported in detail.

A.R.C. C.P.942
April, 1966
J. H. Whitelaw

AN EXPERIMENTAL INVESTIGATION OF THE TWO-DIMENSIONAL WALL JET

A new apparatus, designed to investigate the effects of slot geometry on the effectiveness of film cooling, is described and new measurements of the impervious wall effectiveness are presented. The measurements were performed in the range $2.24 \leq m \leq 0.47$ using helium as a tracer gas and gas chromatographic equipment to detect the relevant concentrations. The appropriate hydrodynamic quantities are reported in detail.

A.R.C. C.P.942
April, 1966
J. H. Whitelaw

AN EXPERIMENTAL INVESTIGATION OF THE TWO-DIMENSIONAL WALL JET

A new apparatus, designed to investigate the effects of slot geometry on the effectiveness of film cooling, is described and new measurements of the impervious wall effectiveness are presented. The measurements were performed in the range $2.24 \leq m \leq 0.47$ using helium as a tracer gas and gas chromatographic equipment to detect the relevant concentrations. The appropriate hydrodynamic quantities are reported in detail.

Printed and published by
HER MAJESTY'S STATIONERY OFFICE

To be purchased from
49 High Holborn, London W C 1
423 Oxford Street, London W 1
13A Castle Street, Edinburgh 2
109 St Mary Street, Cardiff
Brazennose Street, Manchester 2
50 Fairfax Street, Bristol 1
35 Smallbrook, Ringway, Birmingham 5
7 - 11 Linenhall Street, Belfast 2
or through any bookseller

Printed in England

S O. Code No 23-9017-42